

Electronic Supplementary Information

Near-Mid-IR HOMO-LUMO gap in amide linked porphyrin-rhodamine dyads

José A. B. Ferreira,^{*a} Vanda V. Serra,^{a,b} Antonio Sánchez-Coronilla,^{a,c} Sónia M. G. Pires,^b Maria A. F. Faustino,^b Artur M. S. Silva,^b Maria G. P. M. S. Neves,^{*b} José A. S. Cavaleiro^b and Sílvia M. B. Costa^a

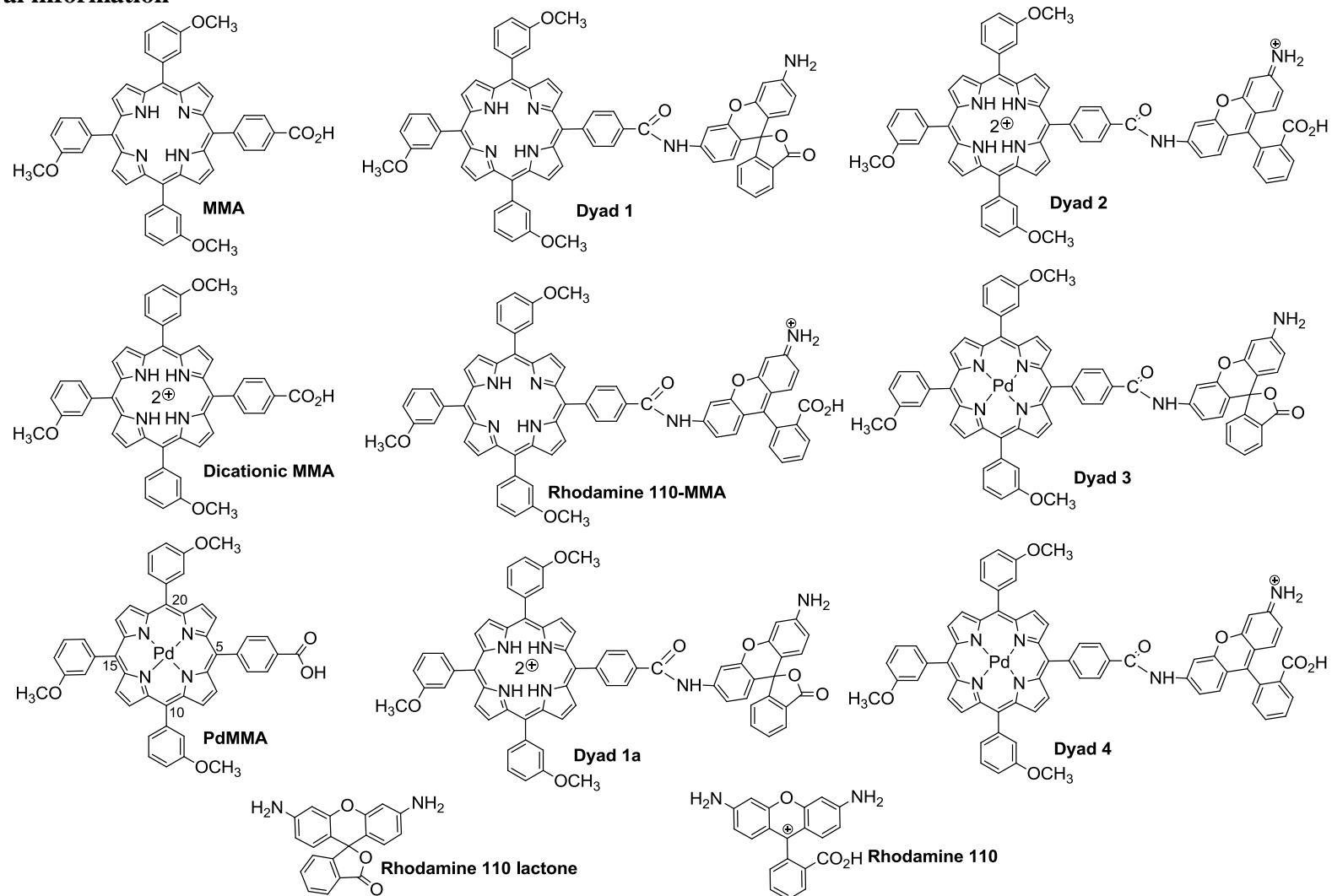
^a *Universidade de Lisboa, Instituto Superior Técnico, Centro de Química Estrutural, Lisbon, Portugal. Fax: +351 218464455; Tel: +351 218419318; E-mail: jose.bracons.ferreira@ist.utl.pt*

^b *Universidade de Aveiro, Departamento de Química, Aveiro, Portugal. Fax: +351 234 370 084; Tel: +351 234 370 710; E-mail: gneves@ua.pt*

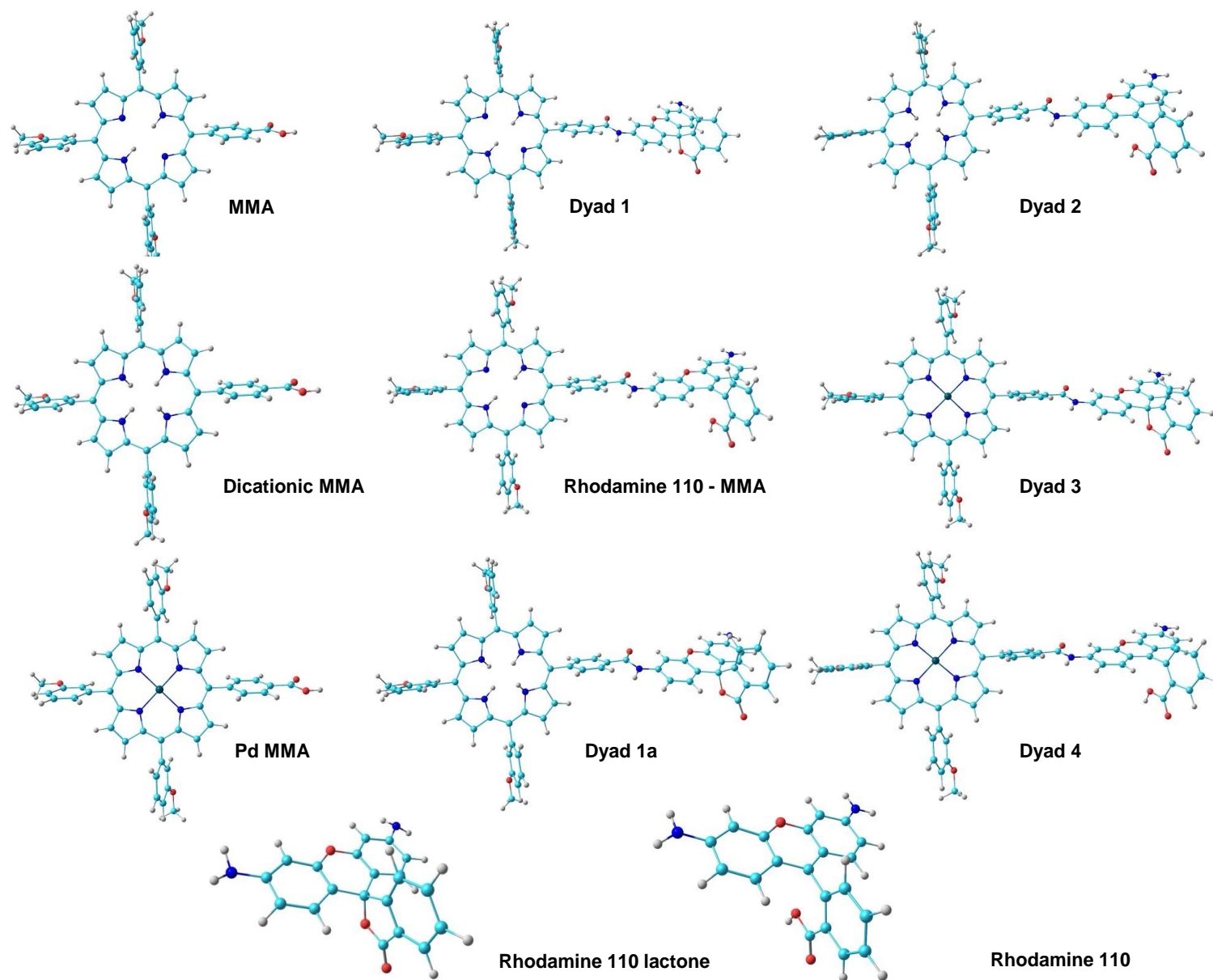
^c *Universidad de Cádiz, Facultad de Ciencias, Cádiz, Spain. Fax: +349 56016288; Tel: +349 56012832; E-mail: antonio.coronilla@uca.es*

Table of contents	2
0 General information	3
Materials and methods	5
Computational details	5
1 Synthesis and structural characterization of Porphyrin - Rhodamine Dyads	6
Dyads 1 and 2	6
Dyads 3 and 4	8
NMR spectra of dyads	9
UV-Vis spectra of dyads	23
2 Theoretical assessments	25
Band gaps	25
Molecular orbitals	25
Transitions energy	26
QTAIM	27
3 References	39

0. General information



Scheme S1 Structures of porphyrins, rhodamines and of porphyrin-rhodamine dyads.



Scheme S2 Optimized structures of porphyrins, rhodamines and of porphyrin-rhodamine dyads.

0.1 Materials and methods

All solvents and reagents were used as received without further purification. The purities of compounds were confirmed by chromatography and NMR spectra. Column chromatography was carried out in silica gel (Merck, 230–400 mesh). Preparative thin-layer chromatography was performed on 20×20 cm glass plates coated with silica gel (0.5 mm thick). Analytical TLC was carried out on pre-coated sheets with silica gel (Merck, 60, 0.2 mm thick). The ^1H and ^{13}C NMR spectra were recorded on a Bruker Avance 300 at 300.13 MHz and 75.47 MHz respectively, using CDCl_3 as solvent and TMS as internal reference. Unequivocal ^1H and ^{13}C assignments were made using 2D COSY, HSQC and HMBC experiments. Mass spectra and HRMS were recorded on VG AutoSpec Q and M mass spectrometers using CHCl_3 as solvent 3-nitrobenzyl alcohol (NBA) as matrix. The UV–Vis spectra were recorded on an UV-2501 PC Shimadzu spectrophotometer using CH_2Cl_2 , CHCl_3 and CHCl_3/TFA as solvents. Uv-Vis-IR spectra were recorded on a Shimadzu UV-3101PC spectrometer using $\text{CCl}_4/\text{CHCl}_3$ and $\text{CCl}_4/\text{CHCl}_3/\text{TFA}$ mixtures as solvents. Uv-Vis-IR spectra of the individual components of the mixtures and respective baselines were acquired to guaranty no spurious interferences especially from moisture.[#]

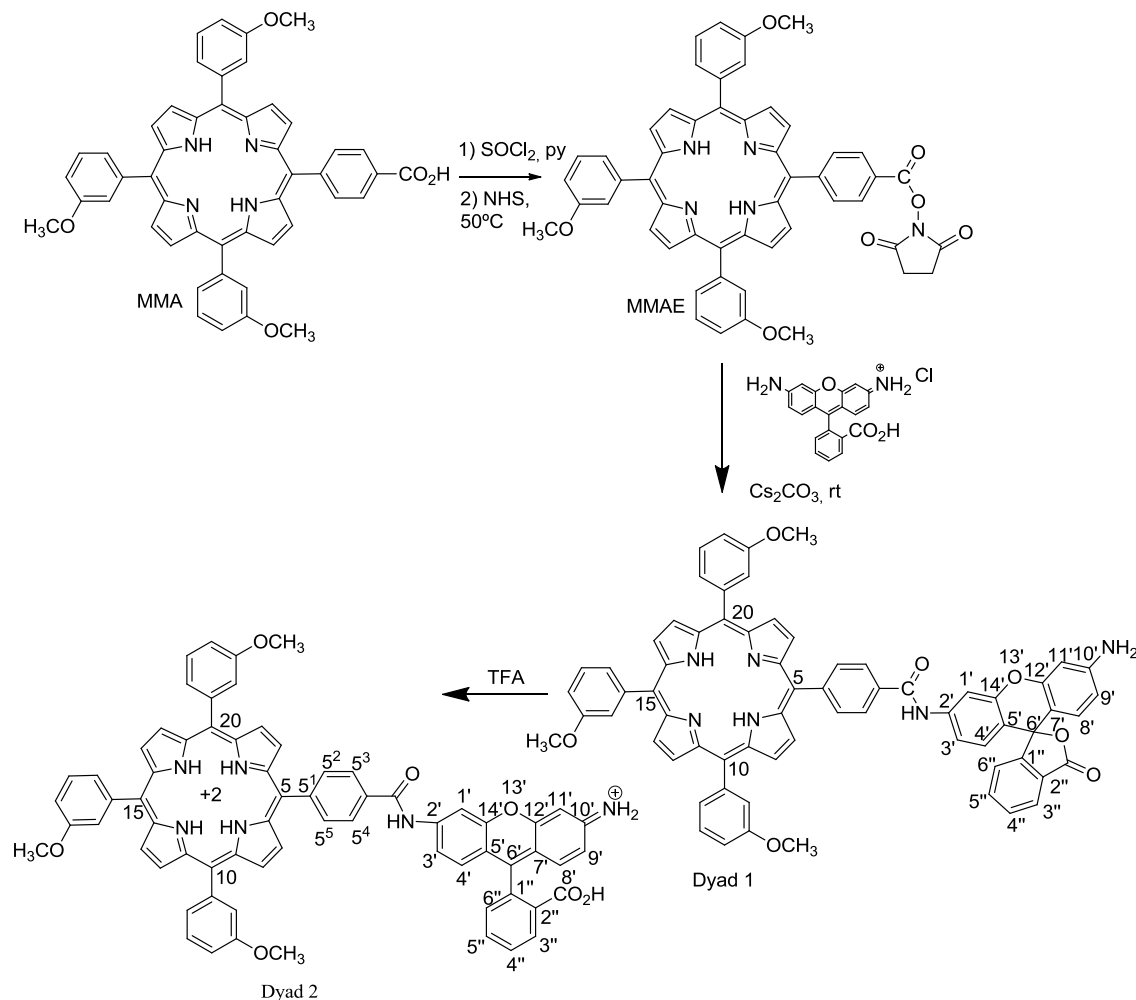
[#] F. M. Nicolaisen, *J. Quant. Spectrosc. & Rad. Trans.*, 2009, **110**, 2060.

0.2 Computational details

Quantum mechanical calculations on the dyadic systems were performed. Computations were carried out using Gaussian 09.¹ Full geometry optimization of the different molecules was performed using Density Functional Theory (DFT) in the context of B3LYP², B97D³, CAM-B3LYP⁴ and LC-BLYP⁵ functionals. The cc-pVDZ basis sets⁶, the pseudopotential LANL2DZ⁷ for Pd and DGDZVP⁸ all electron basis sets were employed. Equilibrium structures were characterized as real minima by calculations of their second derivatives. The geometries obtained were similar with all functionals. Thus, the B3LYP functional, previously used in studies of porphyrins⁹ and rhodamines¹⁰ derivatives, was selected for the general description. If not explicitly mentioned, calculations were performed for isolated molecules without any solvent environment. The time-dependent density functional theory (TDDFT)¹¹ was used to obtain absorption wavelengths and the oscillator strengths (f). The solvent effect was considered using the integral equation formalism (IEF) of the polarisable continuum model (PCM).¹² Wavefunction analysis was carried out by using the atoms in molecule approach by Bader (AIM)¹³ as implemented in the AIMAll software package.¹⁴ For AIM analysis, it was used the DGDZVP all electron basis set. Orbital visualization was performed using Chemcraft 1.6.¹⁵

1. Synthesis and structural characterization of Porphyrin-Rhodamine – Dyads

1.1 Dyads 1 and 2



Scheme S3 Synthesis steps of porphyrin-rhodamine dyads.

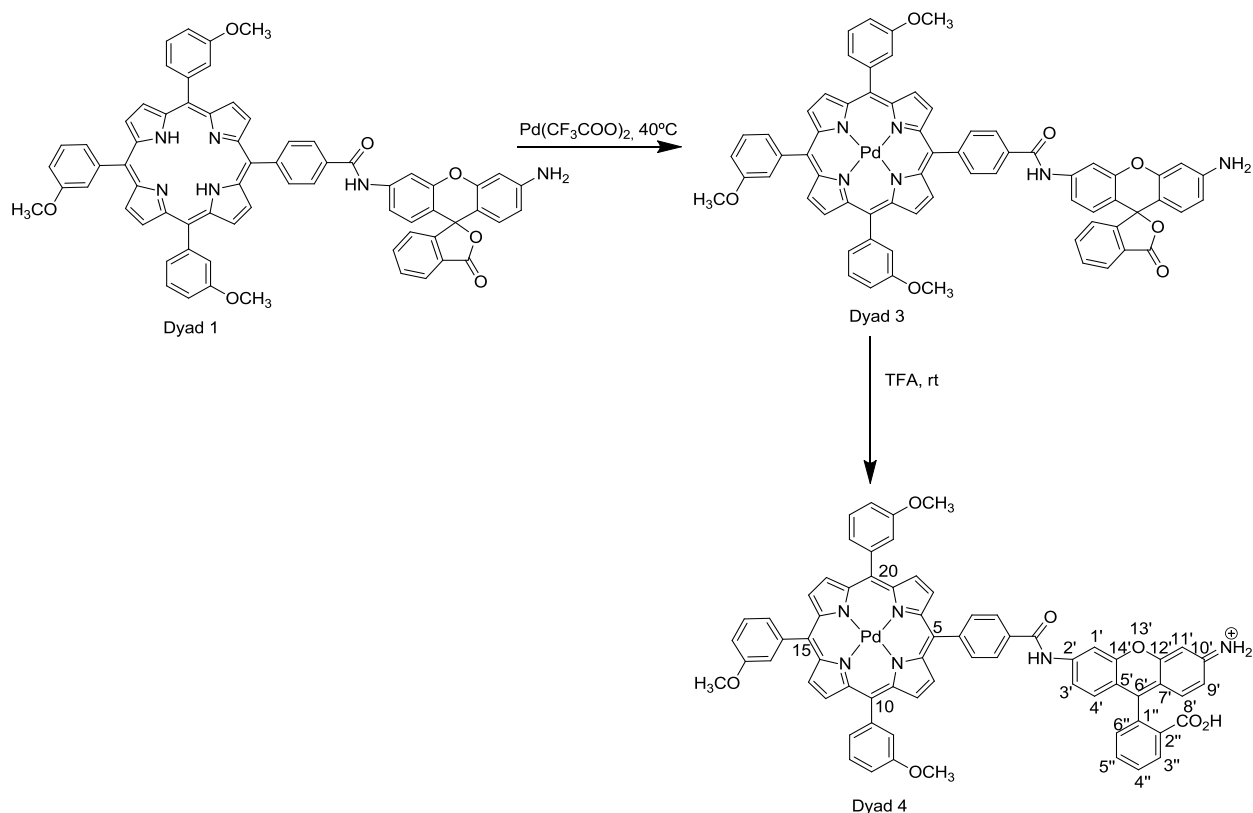
5-(4-carboxyphenyl),10,15,20-tris(3-methoxyphenyl)-porphyrin (**MMA**), and its activated ester (**MMAE**), were prepared according to previously described procedures.¹⁶ To a solution of the activated ester **MMAE** (15.0 mg, 18.0 μmol) in DMSO recently opened (1 ml) was added 3,6-diamino-9-[2-(carboxy)phenyl]-9*H*-xanthen-9-ylidium hydrochloride acid (rhodamine 110, 10 mg, 0.03mmol) and an excess of CsCO_3 anhydrous (10 equivalents). The reaction was kept 24 hours at 25°C , under stirring and protected from light and moisture with silica gel. After total consumption of the starting material, confirmed by TLC, the reaction mixture was dissolved in CH_2Cl_2 and the organic phase extensively washed with water. The recovered organic layer was dried over anhydrous sodium sulfate and evaporated under

reduced pressure. The obtained residue was then dissolved in CH_2Cl_2 and Dyad **1** was purified by preparative chromatography using a mixture of solvents, $\text{CH}_2\text{Cl}_2/\text{MeOH}$ (4%). After crystallization in a $\text{CH}_2\text{Cl}_2/\text{hexane}$ (5:2) mixture, Dyad **1** was isolated pure, 70 % yield. Dyad **2** was obtained quantitatively by addition of a drop of TFA to a 1.0 mM solution of Dyad **1** in CHCl_3 .

Dyad 1 ^1H NMR (CDCl_3), δ (ppm): -2.80 (s, 2H, NH), 3.97 (s, 9H, 10,15,20- OCH_3), 6.29 (dd, $J=2.2$ and $J=8.5$ Hz, 1H, H-9'), 6.51 (d, $J=2.2$ Hz, 1H, H-11'), 6.57 (d, $J=8.5$ Hz, 1H, H-8'), 6.81 (d, $J=8.5$ Hz, 1H, H-4'), 7.21 (d, $J=6.8$ Hz, 1H, H-6''), 7.23 (dd, $J=2.1$ e $J=8.5$ Hz, 1H, H-3'), 7.31-7.34 (m, 3H, 10,15,20- $\text{H}_p\text{-Ar}$), 7.58-7.67 (m, 5H, H-4'', H-5'', 10, 15, 20- $\text{H}_m\text{-Ar}$), 7.77-7.80 (m, 6H, 10,15,20- $\text{H}_o\text{-Ar}$), 8.02 (d, $J=2.1$ Hz, 1H, H-1'), 8.03 (d, $J=7.4$ Hz, 1H, H-3''), 8.24 (d, $J=8.2$ Hz, 2H, 5- $\text{H}_m\text{-Ar}$), 8.31 (d, $J=8.2$ Hz, 2H, 5- $\text{H}_o\text{-Ar}$), 8.39 (s, 1H, COO-NH), 8.77 ($J=5.1$ Hz, 2H, H- β), 8.89 (s, 4H, H- β), 8.90 (d, $J=5.1$ Hz, 2H, H- β). ^{13}C NMR (CDCl_3), δ (ppm): 55.5 ($-\text{OCH}_3$), 84.2 (C-6'), 101.5 (C-11'), 108.3 (C-1', C-7'), 111.7 (C-9'), 113.5, 115.1 (C-5'), 115.5 (C-3'), 118.3, 120.2, 120.1, 120.5, 124.1 (C-6''), 125.0 (C-3''), 125.6, 126.8, 127.5, 127.6, 128.8 (C-4'), 129.1 (C-8'), 129.7, 133.78, 134.8 (5- $\text{C}_o\text{-Ar}$), 135.1 (C-1''), 139.9 (C-2'), 143.3, 146.2, 148.8 (C-10'), 152.1 (C-14'), 152.5 (C-12'), 153.2 (C-2''), 157.9, 165.9 (CO-O), 169.8 (NH-CO). HRMS-ESI m/z for $\text{C}_{68}\text{H}_{49}\text{N}_6\text{O}_7$ ($\text{M}+\text{H}$)⁺ calc. 1061.36170 found 1061.36572. UV-Vis (CH_2Cl_2), λ_{max} (nm): 419 (100%), 514 (4.3 %), 549 (1.6 %), 589 (1.1 %), 644 (0.6%).

Dyad 2: ^1H NMR (CDCl_3/TFA), δ (ppm): -1.48 (s, 4H, NH), 4.18 (s, 9H, 10,15,20- OCH_3), 6.99 (dd, $J=2.0$ and $J=9.4$ Hz, 1H, H-9'), 7.06 (d, $J=2.0$ Hz, 1H, H-11'), 7.29 (d, $J=9.4$ Hz, 1H, H-8'), 7.43 (d, $J=8.8$ Hz, 2H, H-4' and H-6''), 7.58-7.61 (m, 3H, 10, 15, 20- $\text{H}_m\text{-Ar}$), 7.90-7.97 (m, 5H, H-4'', H-5'', 5,10,15- $\text{H}_p\text{-Ar}$), 8.04 (dd, $J=1.9$ and $J=8.8$ Hz, 1H, H-3') 8.10-8.14 (m, 6H, 10,15,20- $\text{H}_o\text{-Ar}$), 8.51-8.56 (m, 4H, H-1', H-3''), 5- $\text{H}_m\text{-Ar}$), 8.71-8.72 (m, 4H, H- β , 5- $\text{H}_o\text{-Ar}$), 8.81 (s, 2H, H- β), 8.71 (d, $J=5.0$ Hz, 4H, H- β) 9.75 (s, 1H, -NH). ^{13}C NMR (CDCl_3), δ (ppm): 56.0 ($-\text{OCH}_3$), 98.7 (C-11'), 108.3 (C-1'), 116.4 (5,10,15- $\text{C}_p\text{-Ar}$), 118.0 (C-7'), 118.4 (C-5'), 120.1 (C-3'), 120.4 (C-9'), 124.1 (5- $\text{C}_m\text{-Ar}$), 127.7 (5- $\text{C}_o\text{-Ar}$), 128.7, 129.3, 129.8 (10,15,20- $\text{C}_m\text{-Ar}$), 130.4 (C-4' and C-6'') 131.4 (C-4''), 131.9 (5,10,15- $\text{C}_o\text{-Ar}$), 132.9 (C-8'), 133.4 (C-3''), 134.8 (C-5'') 138.3, 146.3 (C-2'), 155.3 (C-14'), 160.3 (C-10'), 162.0 (C-5 and C-2''), 169.0 (NH-CO), 170.5 (COOH). UV-Vis (CHCl_3/TFA (1.5 μM)), λ_{max} (nm): 445 (100%), 500 (15.2%), 601 (3.4 %), 654 (15.7 %).

1.2. Dyads 3 and 4



Scheme S4 Synthesis steps of palladium porphyrin-rhodamine dyads.

6.0 mg of Dyad 1 (5.79 mmol) were added to a stirred solution of $\text{Pd}(\text{CF}_3\text{COO})_2$ (13.3 mg, 40.0 μmol , 6.9 equiv.) in a mixture of $\text{CHCl}_3/\text{CH}_3\text{OH}$ (3:1). The reaction mixture was kept under stirring at 40°C and protected from light until complete consumption of Dyad 1 (2 hours as indicated by TLC). The reaction mixture was allowed to reach room temperature, diluted with chloroform and then it was washed with water. The organic solution was dried (Na_2SO_4) and concentrated under reduced pressure. Dyad 3 was obtained pure after precipitation in a CHCl_3/n -hexane mixture. Dyad 4 was obtained qualitatively after addition of a drop of TFA to a 1.0 mM solution of Dyad 3 in CHCl_3 .

Dyad 3: HRMS-ESI m/z for $\text{C}_{68}\text{H}_{46}\text{N}_6\text{O}_7\text{Pd}$ ($\text{M}+\text{H}$)⁺ calc. 1165.25411 found 1165.25575.

UV-Vis (CHCl_3), λ_{max} (nm): 467 (100%), 573 (13 %).

Dyad 4: UV-Vis (CHCl_3/TFA (5 μM)), λ_{max} (nm): 467 (100%), 525 (13 %), 571 (15 %).

1.3. NMR spectra of Dyads

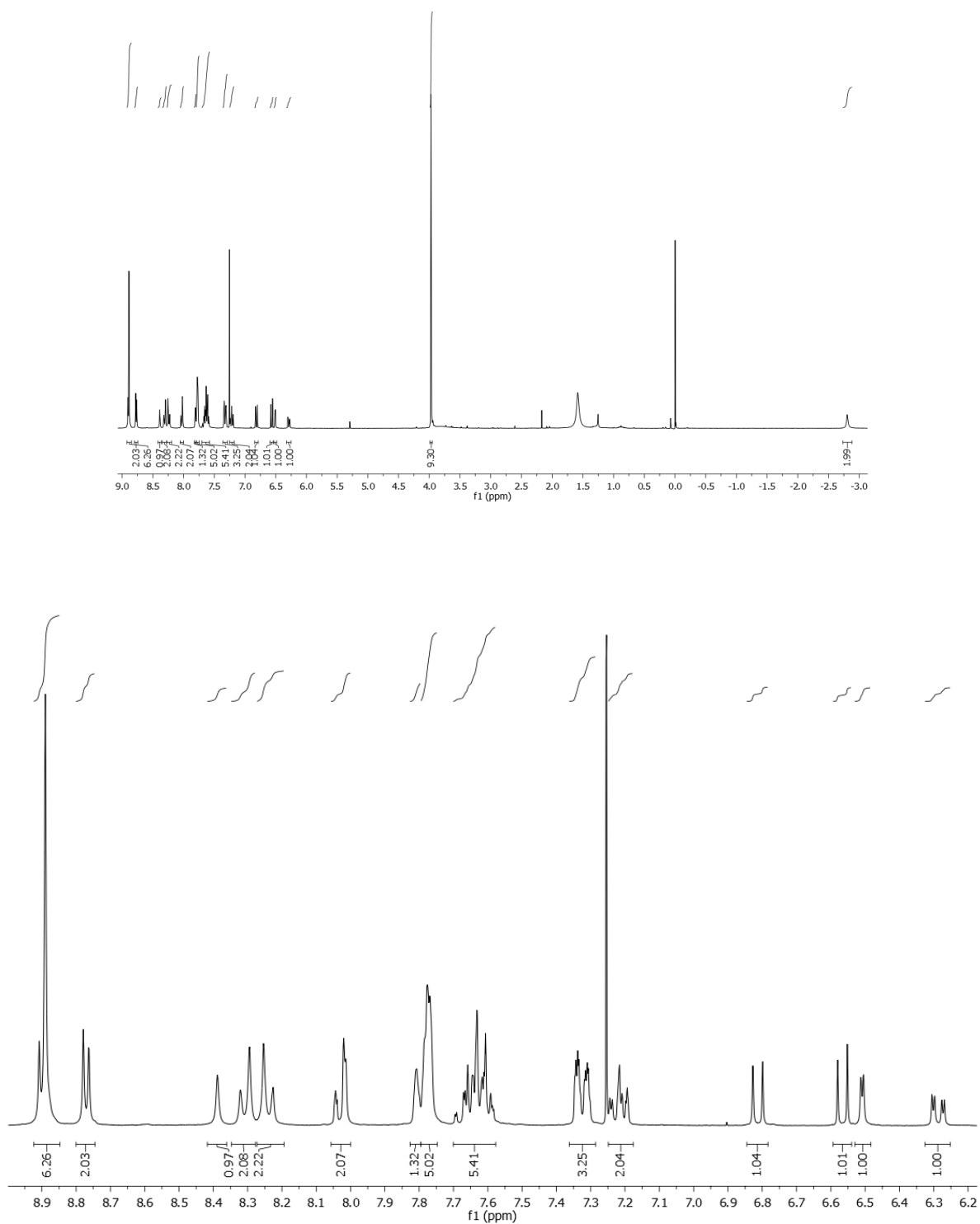


Figure S1 ^1H NMR spectrum of Dyad 1.

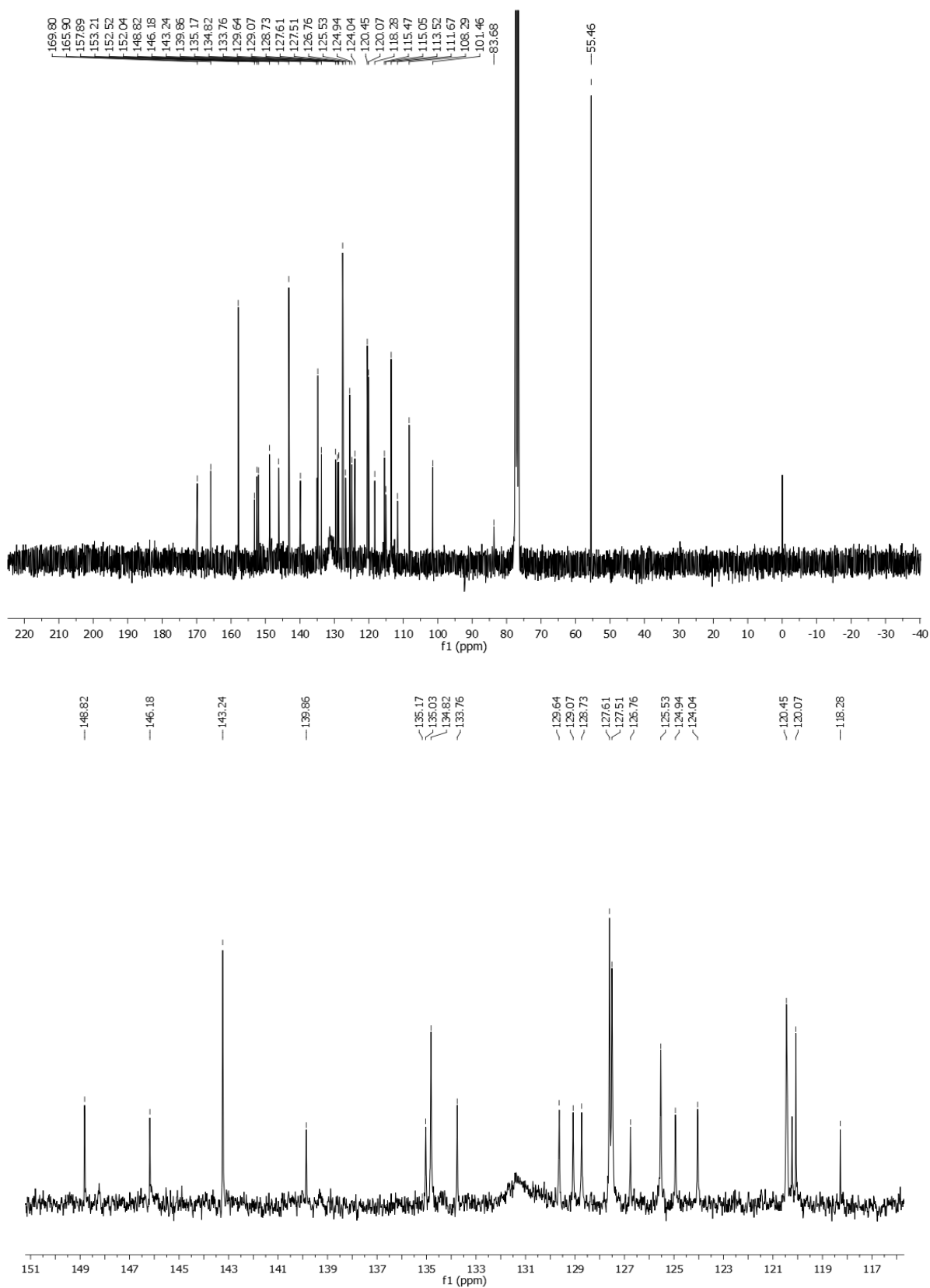


Figure S2 ^{13}C NMR spectrum of Dyad 1.

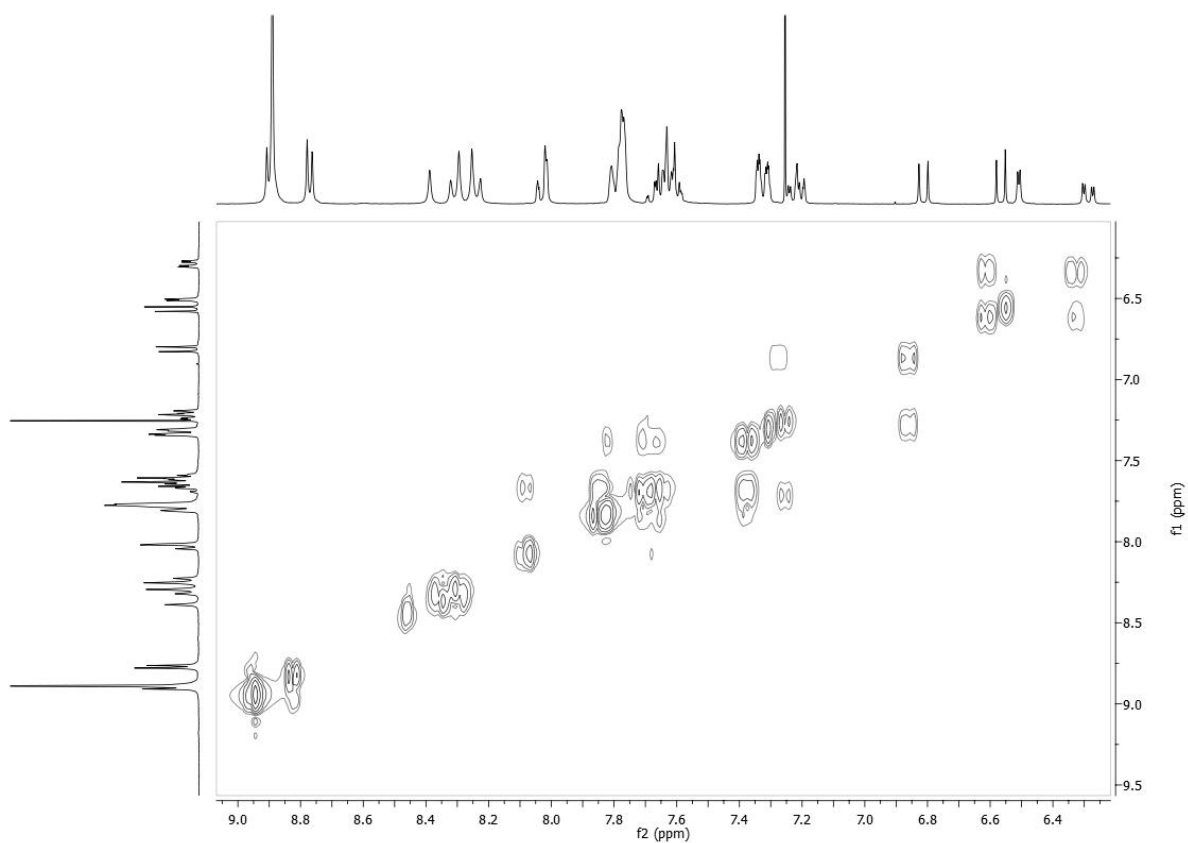


Figure S3 COSY spectrum of Dyad 1.

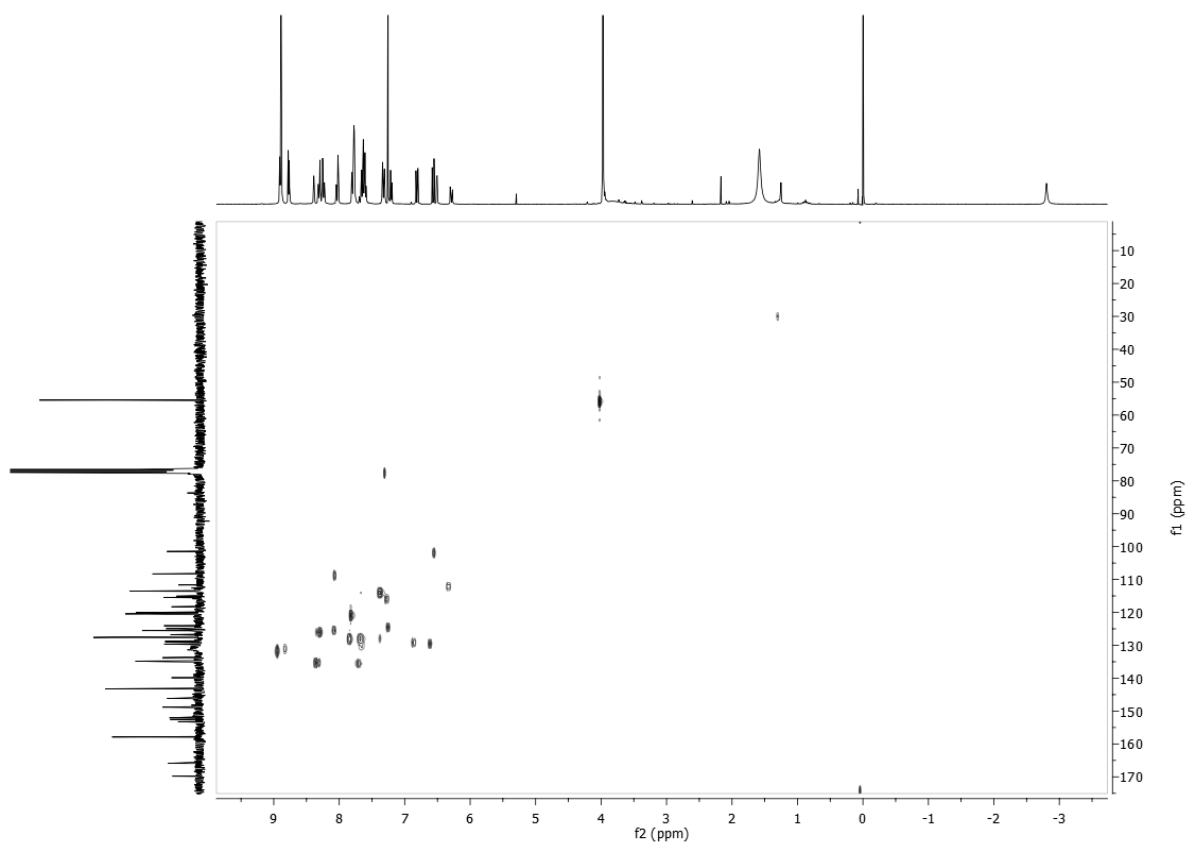


Figure S4 HSQC spectrum of Dyad 1.

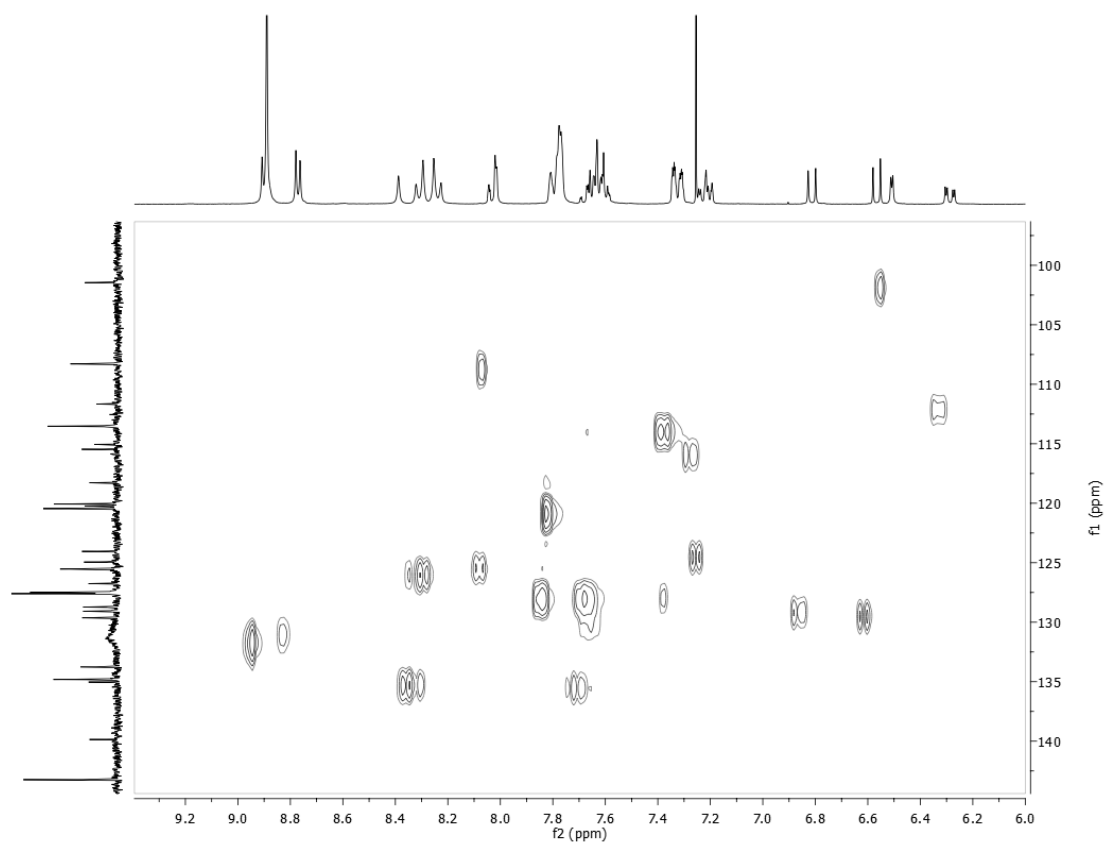


Figure S5 HSQC spectrum of Dyad **1**.

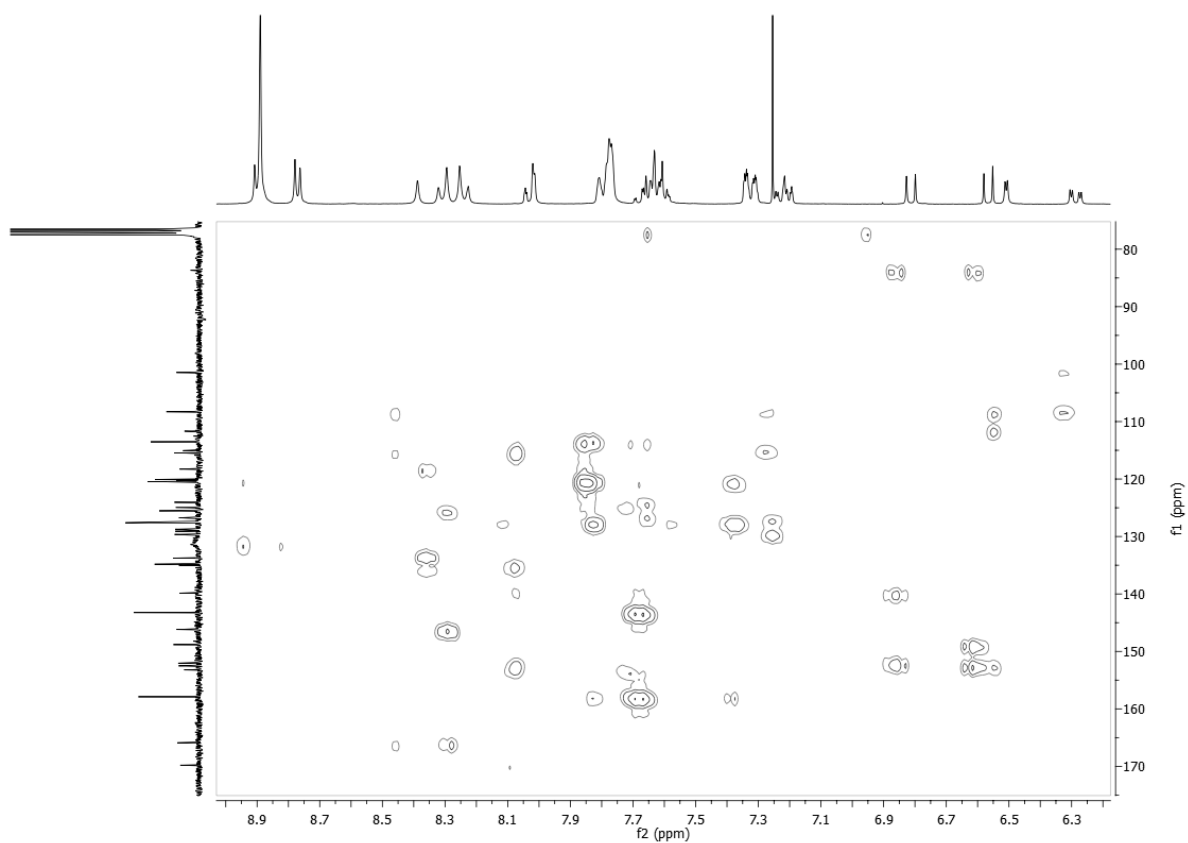


Figure S6 HMBC spectrum of Dyad 1.

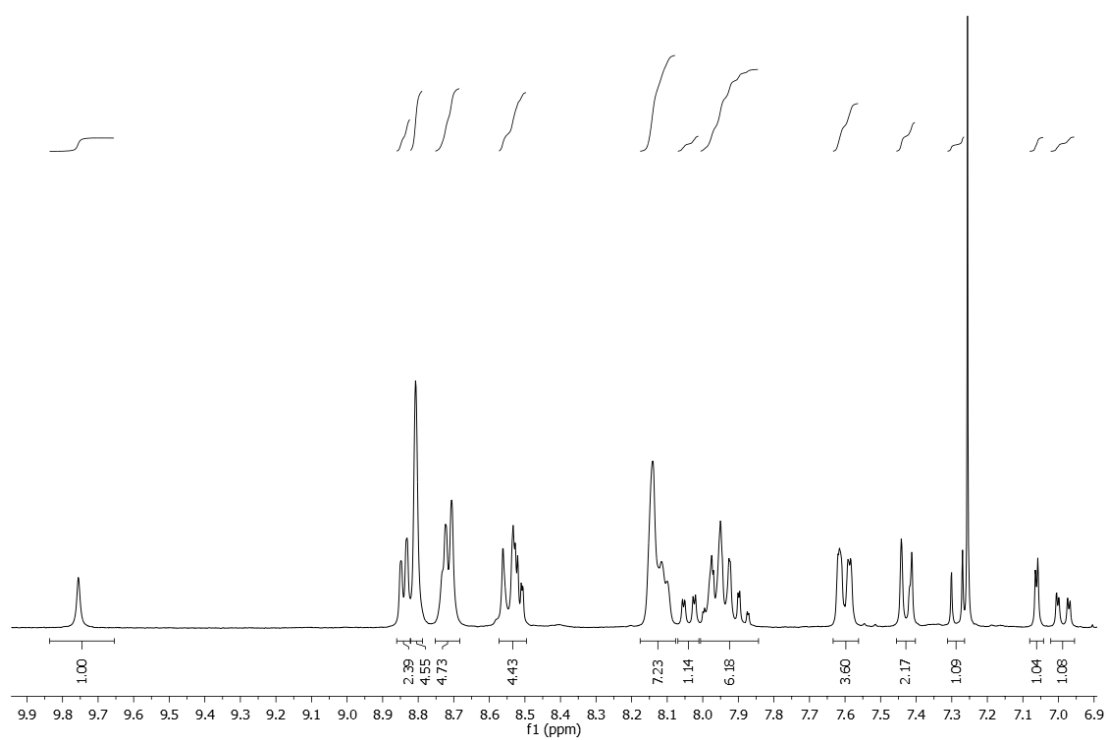
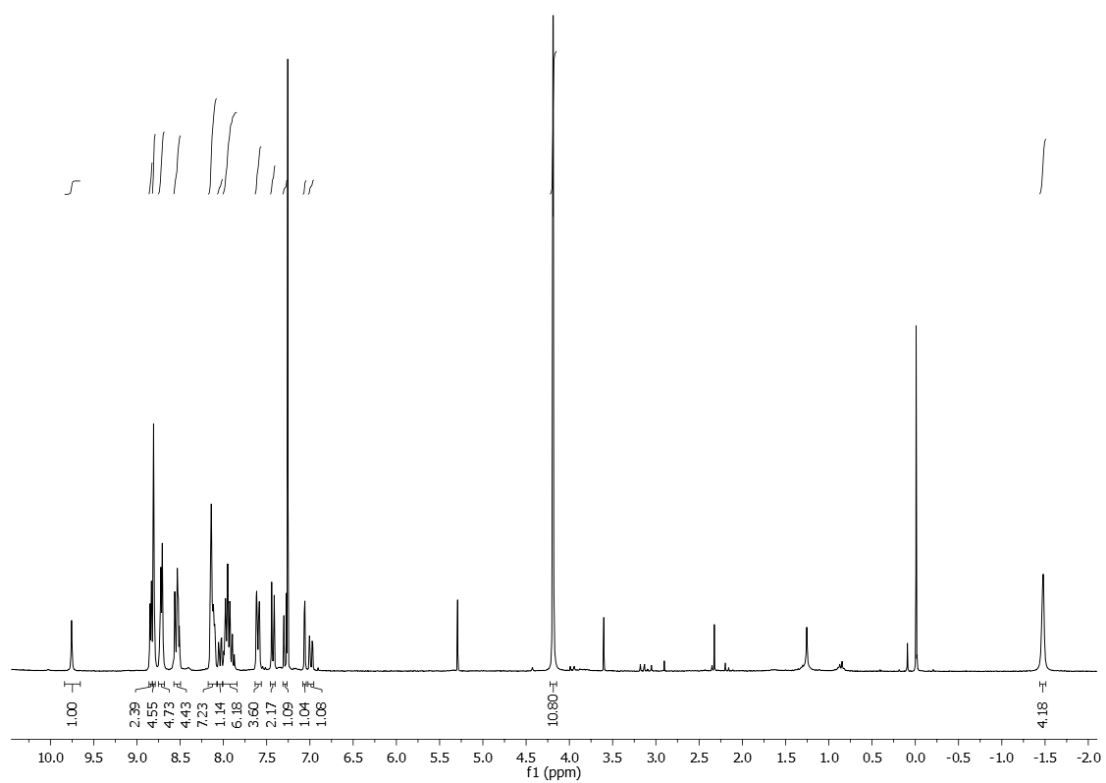


Figure S7 ^1H NMR spectrum of Dyad 2.

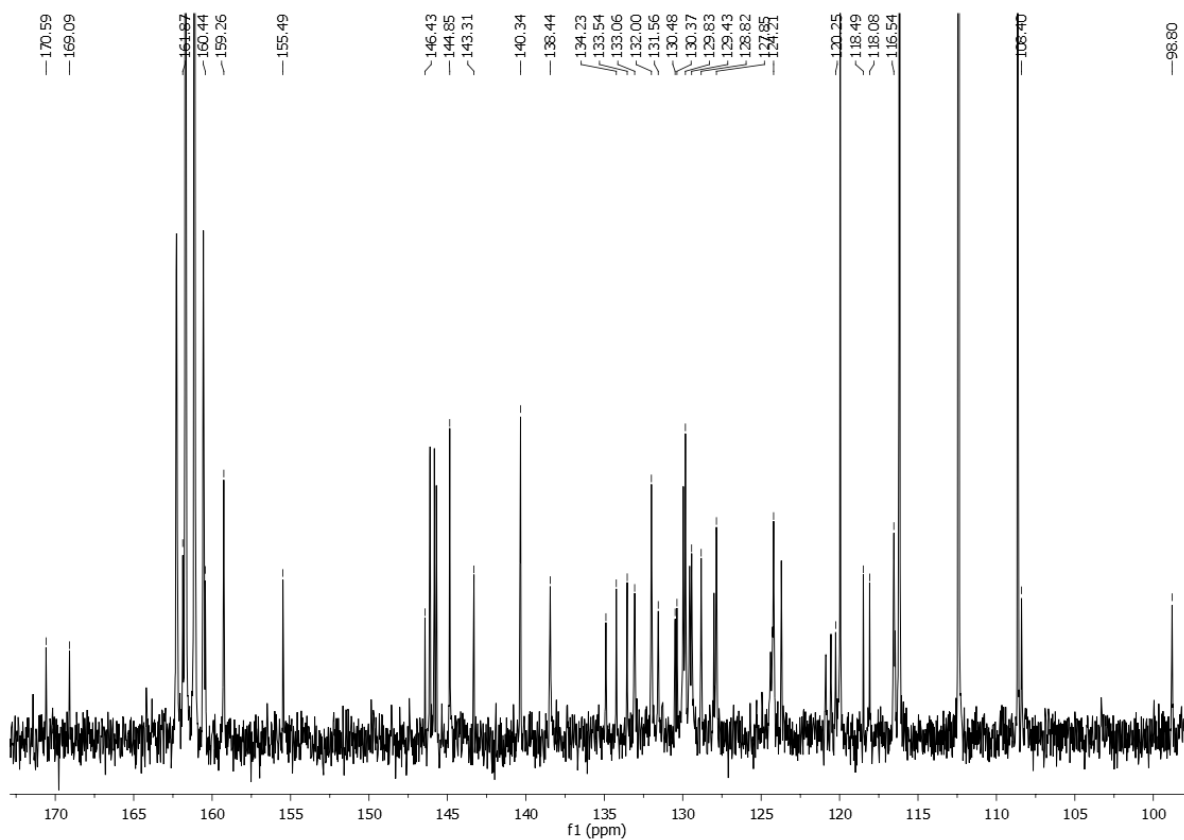
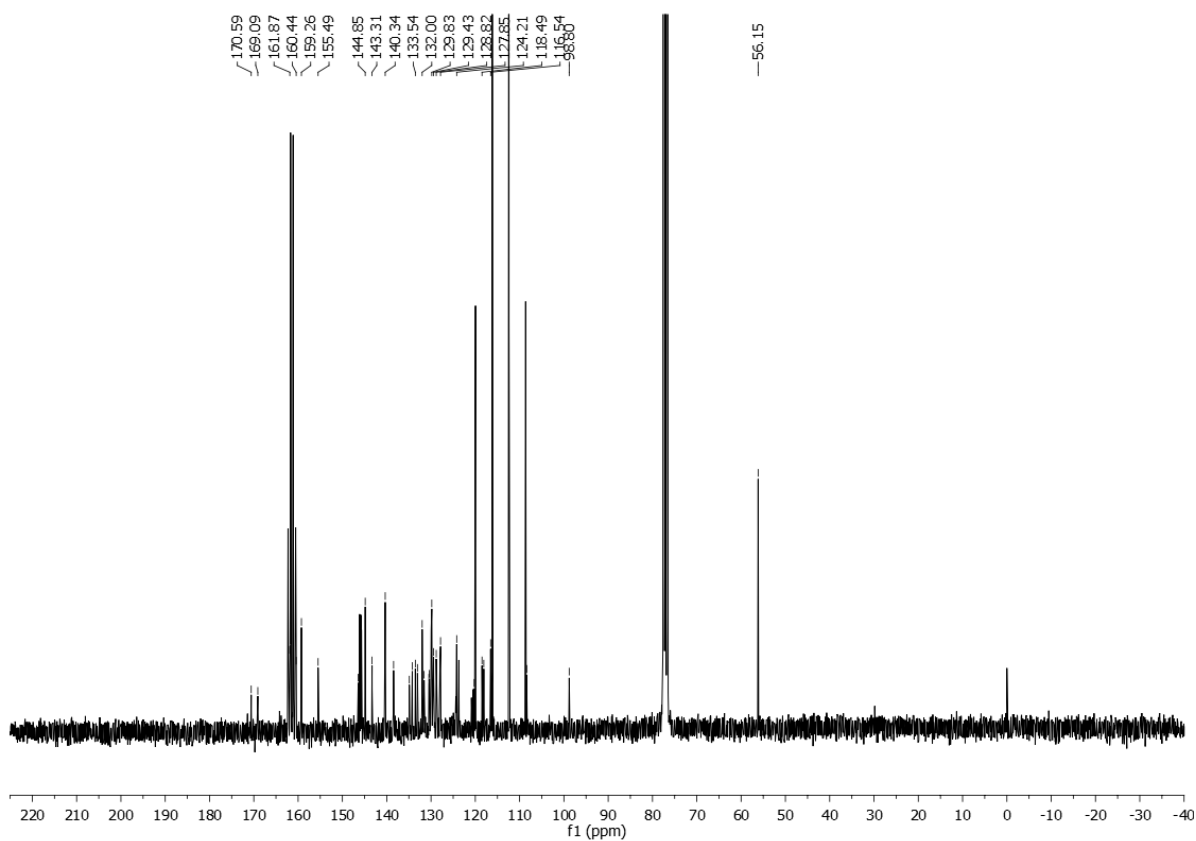


Figure S8 ^{13}C NMR spectrum of Dyad 2.

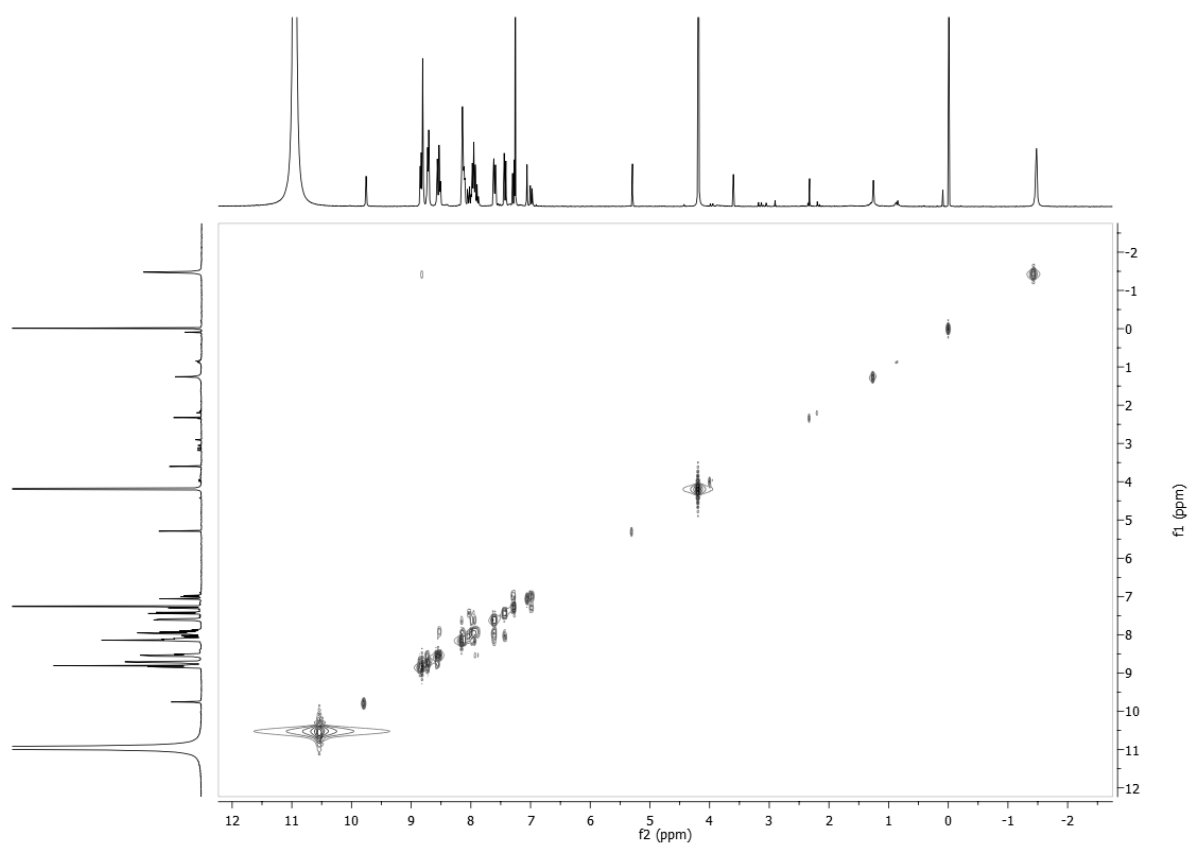


Figure S9 COSY spectrum of Dyad **2**.

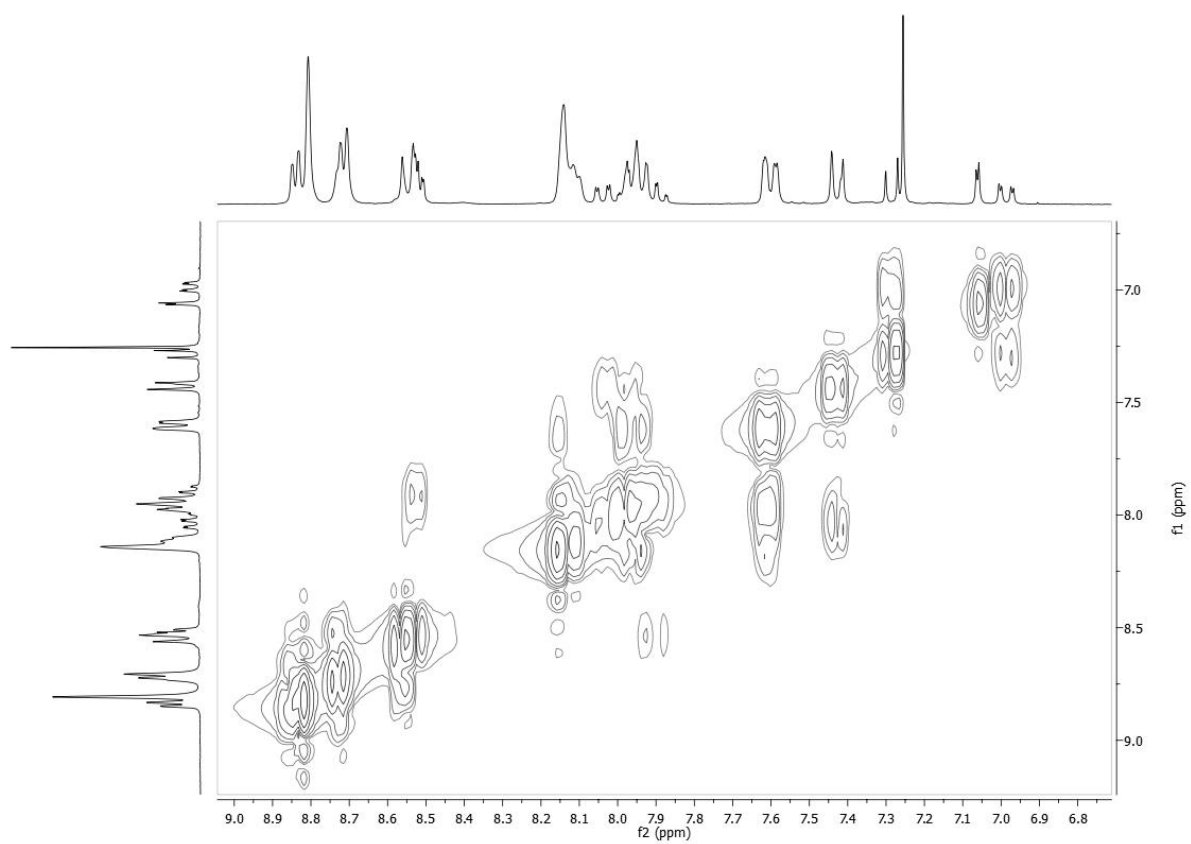


Figure S10 COSY spectrum of Dyad 2.

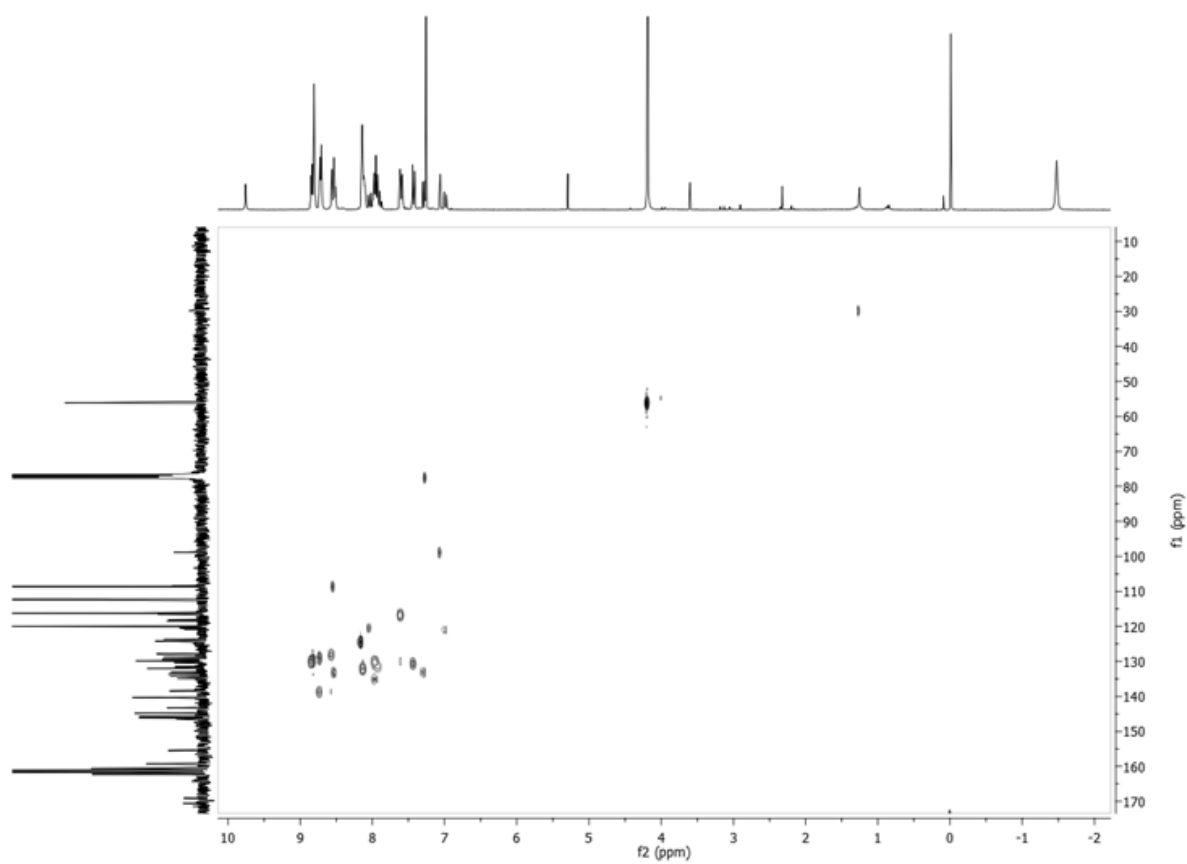


Figure S11 HSQC spectrum of Dyad **2**.

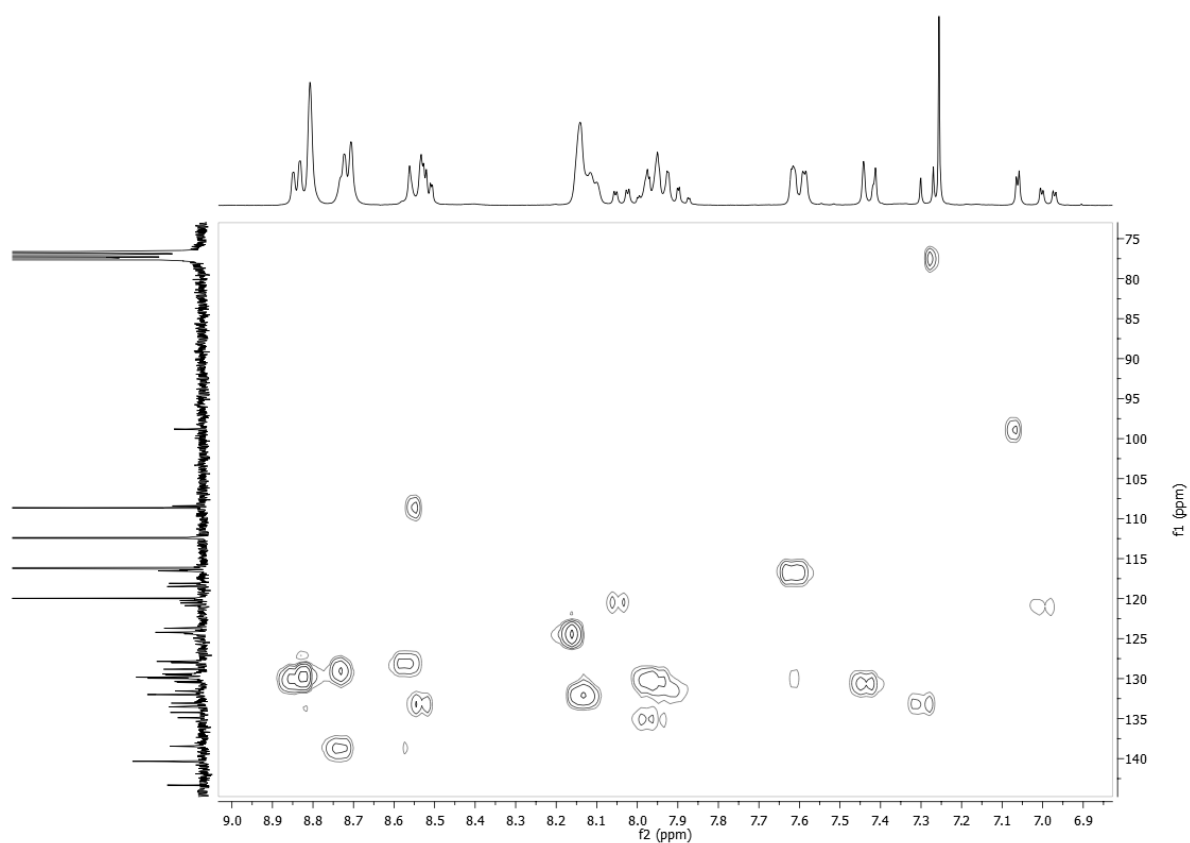


Figure S12 HSQC spectrum of Dyad 2.

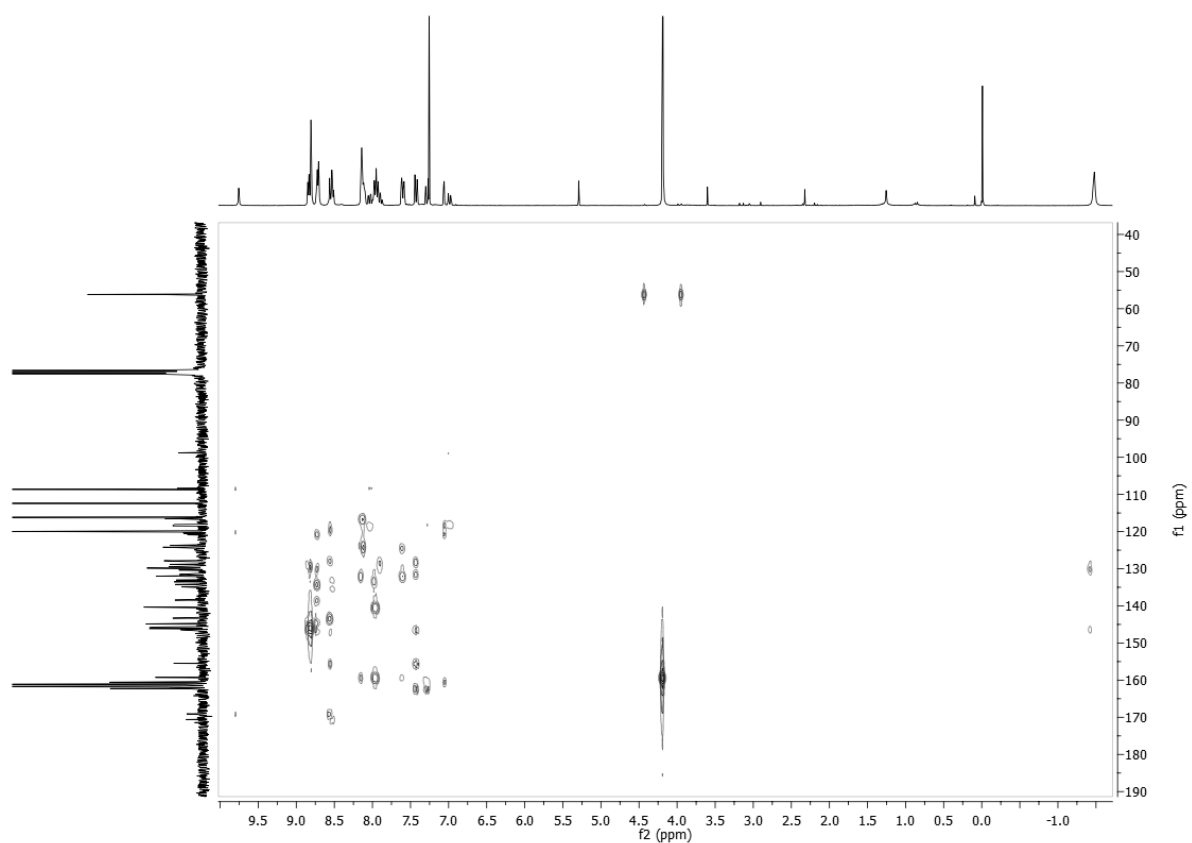


Figure S13 HMBC spectrum of Dyad **2**.

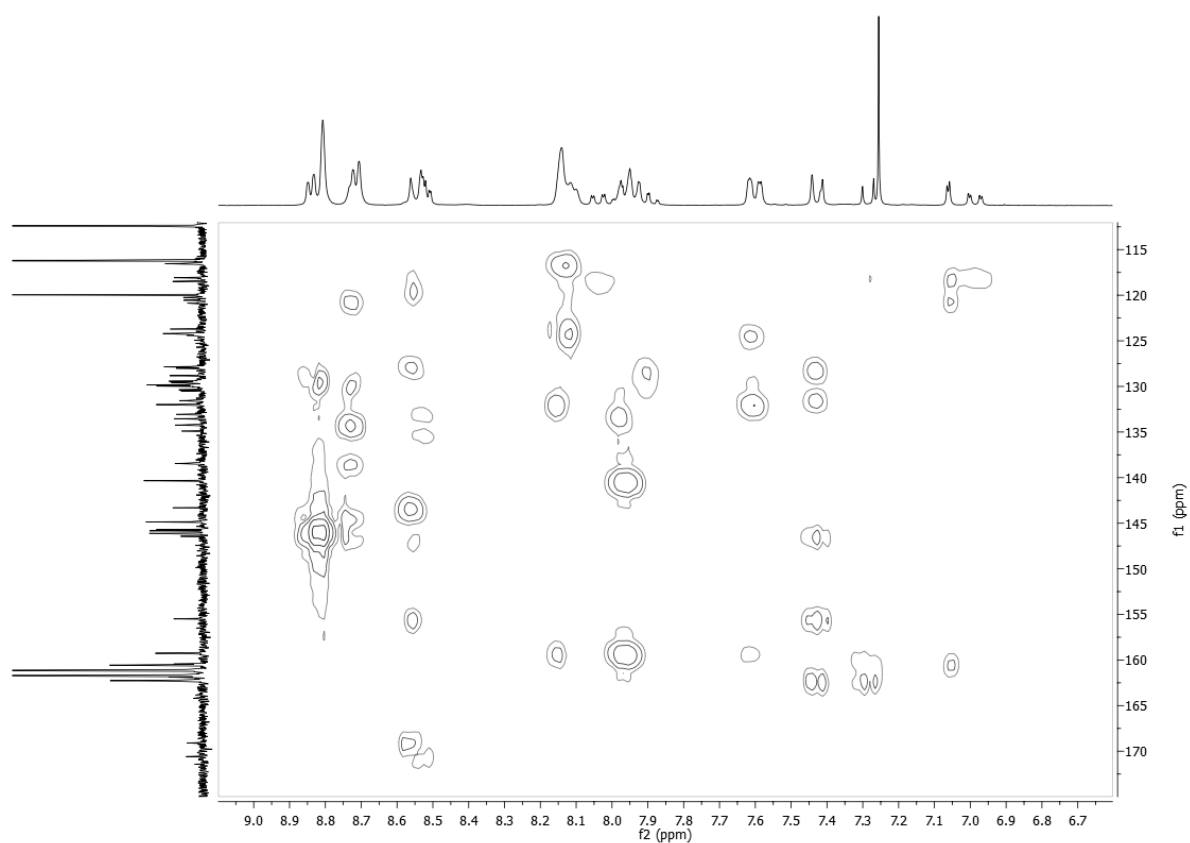


Figure S14 HMBC spectrum of Dyad 2.

1.4 UV-Vis spectra of Dyads

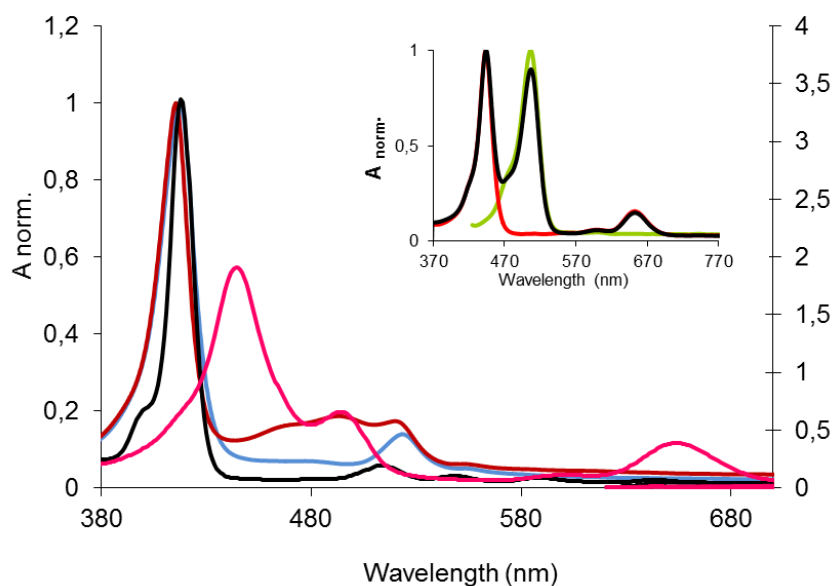


Figure S15 UV-Vis spectra of Dyads: **1** in CHCl_3 (-), **2** in CHCl_3/TFA ($5 \mu\text{M}$) (-), **3** in CHCl_3 (-), and **4** in CHCl_3/TFA ($5 \mu\text{M}$) (-). Inset: Spectra of individual chromophoric units in CHCl_3/TFA ($5 \mu\text{M}$): Dicationic MMA (-), rhodamine 110 methyl ester (-) and mixture of dicationic MMA and rhodamine 110 methyl ester (-).

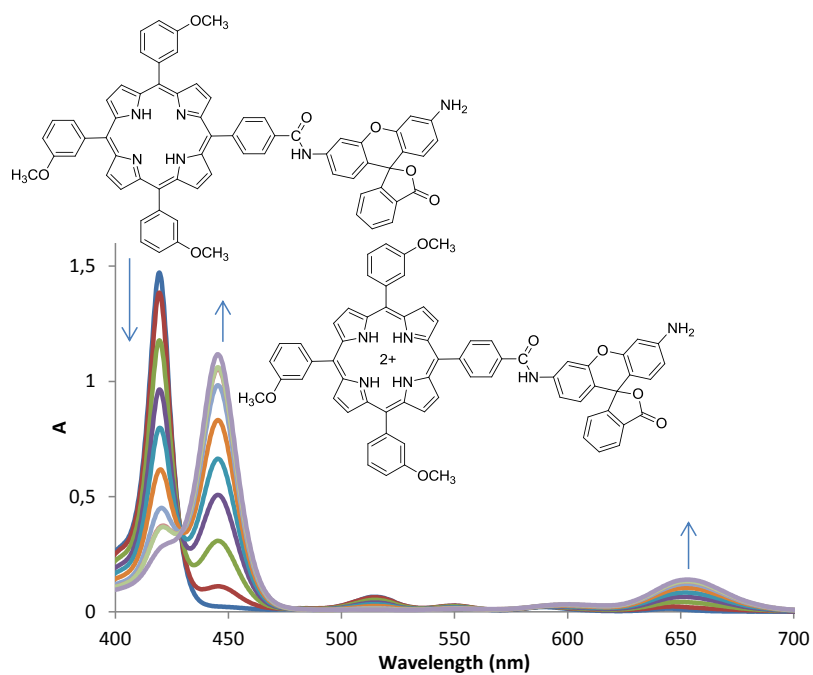


Figure S16 UV-Vis spectra of Dyads **1** and **1a** in CHCl_3/TFA (0 - $0.5 \mu\text{M}$).

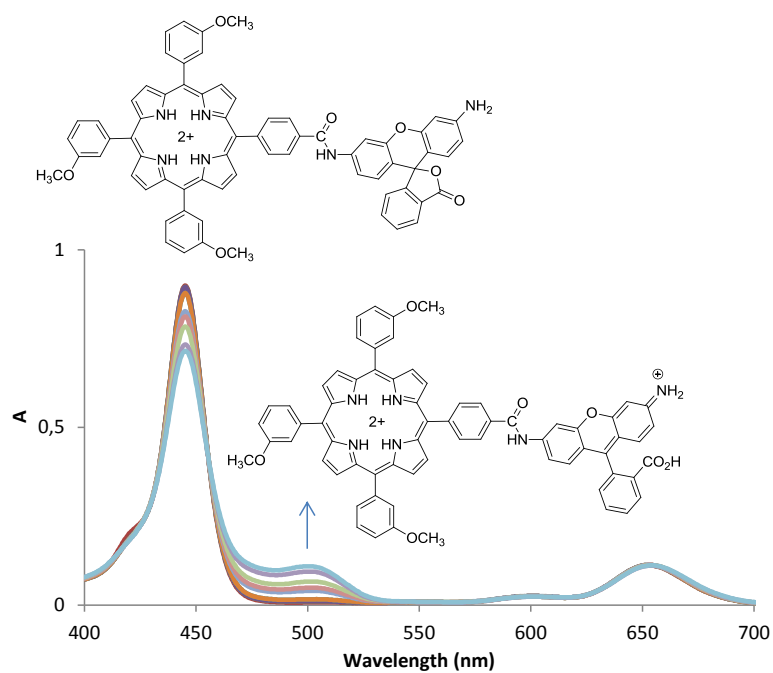


Figure S17 UV-Vis spectra of Dyads **1a** and **2** in CHCl_3/TFA (0.5 - 1.5 μM).

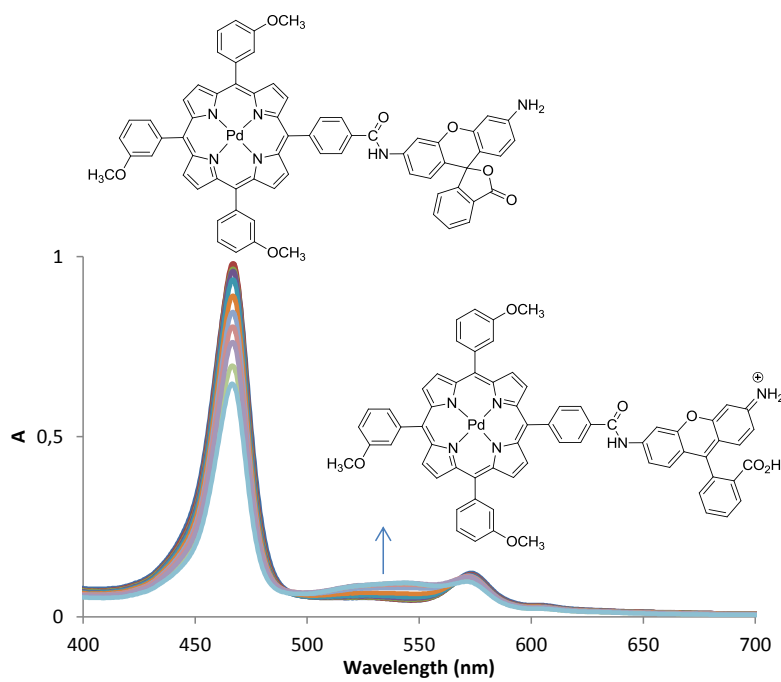


Figure S18 UV-Vis spectra of Dyads **3** and **4** in CHCl_3/TFA (0 - 5 μM).

2 Theoretical assessments

Molecular orbitals, transitions energies in gas phase and in presence of solvents, complete energy bands description and interpretation of band gaps as well as the molecular electrostatic potentials were achieved considering the molecular precursors, moieties and dyads including a model dyadic system that has been designed since its experimental counterpart is not accessible. The theoretical results predict IR absorption bands in agreement with experimental results. IR absorption is generated by an electron transfer process associated to the HOMO→LUMO transition where the π -delocalization of the system plays a crucial role that is addressed through the ellipticity analysis. The HOMO→LUMO transitions that give the lowest band gap energies involve the porphyrin subunits (HOMO) and the diaminoxanthenic (LUMO) moieties. Quantum Theory of Atoms in Molecules was employed to assess the ellipticities at bonds critical points in the amide linkage considering its dominant role in the novel dyads.

2.1 Band gaps Theoretical results predict higher band gap energy in Dyad **1** as compared to that of the dyadic model structure Rhodamine 110 - MMA, regardless of the level of calculation. In turn, we will discuss the similarities and differences that both Rhodamine 110 and Rhodamine 110 lactone moieties have in their particular systems. The main difference between these two dyadic structures is in the rhodamine moieties. The band gap of Rhodamine 110 is *c.a.* 1.3 eV lower than that of Rhodamine 110 lactone (Figure S19).

Figure S19

2.2 Molecular orbitals The HOMOs of both structures are located on the diaminoxanthenic moiety with a π character, similar to that reported elsewhere¹⁷ for other rhodamine derivatives. By contrast, LUMO of Rhodamine 110 lactone is located on the phenyl substituent, while the LUMO of Rhodamine 110 is located in the diaminoxanthenic moiety and only partially located in the phenyl ring, Figure S20. The MMA HOMO and LUMO are located mainly on the porphyrin ring¹⁸ with π and π^* character, respectively, Figure S21. Rhodamine 110 HOMO and LUMO energies are lower than those of MMA. In the case of Dyad **1**, the band gap is similar to that of MMA, *c.a.* 2.7 eV. Thus, the HOMO and LUMO belong mainly to the porphyrin moiety in the dyad. This result is also attested by the molecular orbital diagram, where the Rhodamine 110 lactone HOMO and LUMO are lower and higher, respectively, than those of MMA. However, in the case of Rhodamine 110 - MMA dyad, its band gap is *c.a.*

0.5 eV, and it is remarkable the crucial role that plays the Rhodamine 110 like moiety. HOMO is mainly located on the porphyrin moiety and the LUMO is mainly located on the diaminoxanthenic ring, which facilitates the electron transfer between the two dyad moieties.

Figure S20. Figure S21

The present discussion focuses now on the comparison of Rhodamine 110 - MMA with Dyad **1** and Dyad **3** and is fully extrapolated to the experimentally observed Dyad **1a** / Dyad **2** and Dyad **3** / Dyad **4**, systems. The molecular orbital contributions indicate the direction of efficient electron transfer in Dyad **4** by contrast to Dyad **3**. The band gap of Dyad **3** is similar to that of the PdMMA, *c.a.* 2.8 eV, and its HOMO and LUMO are located on the porphyrin moiety. In Dyad **4** the HOMO is located on the porphyrin subunit that acts as donor¹⁹, and the LUMO is mainly located on the Rhodamine 110 like moiety that acts as acceptor subunit. A similar scenario is also observed for the Dyad **1a** / Dyad **2**. In Dyad **1a**, the HOMO and LUMO are located on the porphyrin moiety, with a band gap similar to that of the dicationic form of MMA, *c.a.* 1.5 eV. In Dyad **2**, the HOMO is essentially located on the porphyrin subunit, and the LUMO is mainly located on the Rhodamine 110 like moiety what also indicates the direction of the efficient electron transfer. We thus confirm that our designed dyes bearing the Rhodamine 110 like subunit are more suitable for electron injection than those bearing the Rhodamine 110 lactone moiety.

2.3 Transitions energy To provide a clear interpretation of spectral changes accompanying the dyads electronic absorption, Time-Dependent Density Functional Theory (TDDFT)¹¹ calculations were performed. Herein we used different DFT methods such as, B3LYP⁶, B97D³, CAM-B3LYP⁴ and LC-BLYP⁵. Our results turn out that B3LYP and B97D functionals provide better agreement with the experimental absorption data than CAM-B3LYP and LC-BLYP methods (Table S1). Therefore we chose the TD-B3LYP and TD-B97D results for further calculations. The solvent effect (CCl₄, $\epsilon = 2.23$, and CHCl₃, $\epsilon = 4.71$) computed by the integral equation formalism (IEF) version of the polarisable continuum model (PCM)¹² is also included on the benchmark calculations to take into account the experimental conditions.

Table S1

The experimental results for Dyad **2** and Dyad **4** show absorption bands at *c.a.* 3100-3200 nm. By comparing the theoretical and the experimental values, it turns out that the better

agreement is found by using the TD-B97D method in presence of CCl₄ as solvent depicting the environment of the system (Table S2). We also include the main composition of the excitation and its oscillator strength.

Table S2

Considering first Dyad **1**, Dyad **1a** and Dyad **3**, at longer wavelengths the only transition that appears corresponds to the well-known Q band of porphyrins.^{18,20,21} This band is mostly described by the HOMO→LUMO transition, what is in agreement with the previous discussion where the MMA, dicationic MMA and PdMMA HOMOs and LUMOs are located mainly on the porphyrinic moiety of the dyads. Concerning dyadic model structure Rhodamine 110 - MMA, Dyad **2** and Dyad **4**, the theoretical results predict absorption bands in the IR region as observed experimentally. Molecular orbitals contributing to transitions in that region are mainly described with HOMO→LUMO transition, with HOMO located on the porphyrin subunit and LUMO mainly located on the Rhodamine 110 like moiety as above previously discussed explaining the reduced energy gap. Agreement with experimental results in what concerns computed absorption wavelengths, are blue-shifted with increasing dielectric constant. No significant shift occurs in Dyad **1**, Dyad **1a** and Dyad **3** by varying the dielectric media. Thus, the displacement observed for dyadic model structure Rhodamine 110 - MMA, Dyad **2** and Dyad **4** indicates the existence of a difference of charge between its subunits as compared to Dyad **1**, Dyad **1a** and Dyad **3** as attested by the mapped surface molecular electrostatic potential (MEP) images (Figure S22) and also by their strongly different dipole moments.

Figure S22

2.4 QTAIM To further gain insight into the electronic properties that underlie the energy effects mentioned above, we will discuss the electronic structures within the framework of the Quantum Theory of Atoms in Molecules (QTAIM).¹³

The QTAIM method is based on the topological analysis of the electron density, ρ , that is dominated by the attractive forces of the nuclei.¹³ When the first derivatives of the density vanish, we have a critical point (cp) in the electron density, and this determines the positions of extrema in ρ (maxima, minima or saddle points). In three dimensions we have three intrinsic curvatures called eigenvalues λ_1 , λ_2 and λ_3 . When ρ is a maximum with λ_1 and λ_2 negatives and λ_3 positive we have a bond critical point (BCP). The ellipticity at the bond

critical point measures the extent to which density is preferentially accumulated and it is defined as:

$$\varepsilon = \frac{\lambda_1}{\lambda_2} - 1 \quad (1)$$

As $\lambda_1 < \lambda_2 < 0$, the ellipticity is always positive. When $\varepsilon = 0$ the bond is cylindrically symmetrical as typically C-C single bond. In doing so, the ellipticity is a concise quantity to characterize electron delocalization and measure the π -character of the bonding in the studied systems. At this point, it is of interest the analysis of the π -character as π -delocalization of the linker between the two moieties in the dyads because it should play an important role in the electron transfer process, (Scheme S5, Table S3).

Scheme S5, Table S3

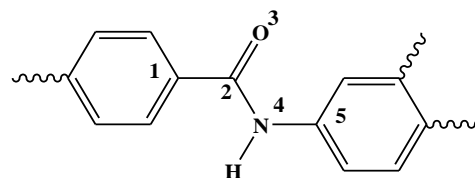
Thus, as shown in Table S3, the ellipticity at the bond critical points of the bond C₁-C₂, C₂-O₃ and N₄-C₅ of dyadic model structure Rhodamine 110 - MMA, Dyad **2** and Dyad **4** are higher than those of Dyad **1**, Dyad **1a** and Dyad **3**. Moreover, when we compare the ellipticity values with their respective precursors (MMA, dicationic MMA, PdMMA, Rhodamine 110 and Rhodamine 110 lactone) we observe an increase in the π -character, $\Delta\varepsilon > 0$, for those bonds in dyadic model structure Rhodamine 110 - MMA, Dyad **2** and Dyad **4** and a decrease, $\Delta\varepsilon < 0$ in Dyad **1**, Dyad **1a** and Dyad **3**. Therefore, there is a π -delocalization in dyadic model structure Rhodamine 110 - MMA, Dyad **2** and Dyad **4** as compared to Dyad **1**, Dyad **1a** and Dyad **3** where their π -character is mainly focused on the C₂-N₄ bond. The observed characteristics are related to the geometrical properties of the linker, in special to the bond length (shorter for the C₁-C₂, C₂-O₃ and N₄-C₅ bonds of dyadic model structure Rhodamine 110 - MMA, Dyad **2** and Dyad **4** because only small differences are appreciated for the dihedral angles (*c.a.* 168° for dyadic model structure Rhodamine 110 - MMA / Dyad **1**, 178° for Dyad **2**/Dyad **1a** and 177° for Dyad **4** / Dyad **3**). Of note is the correlation we found between the ellipticities and the photophysical properties that resembles those reported elsewhere for phenyl-terpyridine compounds.²² Our theoretical results predict that the dyads with lowest band gap energy which absorb at the IR are those with higher ellipticity in the linker bridge that extends the π -system and enhances the π -delocalization, Figure S23.

Table S1 Selected excitation wavelengths, λ , and oscillator strengths, f , for the optical transitions in gas phase
 (level: cc-pVDZ and LANL2DZ for Pd).

NAME	Functional							
	B3LYP		B97D		CAM-B3LYP		LC-BLYP	
	λ (nm)	f						
MMA	578.32	0.0169	632.35	0.0371	536.51	0.0154	518.42	0.0110
Dicationic MMA	607.64	0.0800	658.08	0.0111	382.03	0.4474	571.66	0.0060
Pd MMA	518.61	0.0275	581.80	0.1011	508.72	0.0112	538.31	0.0035
Rhodamine 110 lactone	320.17	0.0051	413.79	0.0027	253.36	0.0213	237.59	0.1449
Rhodamine 110	408.70	0.5918	449.99	0.4159	379.49	0.7368	358.32	0.8432
Dyad 1	578.32	0.0169	632.72	0.0471	536.67	0.0181	518.51	0.0119
Rhodamine 110 - MMA	3534.69	0.0832	3285.72	0.1669	739.89	0.0234	520.00	0.0109
Dyad 1a	615.86	0.1002	656.39	0.0078	381.90	0.5134	551.04	0.0034
Dyad 2	2871.47	0.0912	2921.09	0.0861	1862.96	0.0511	581.26	0.0218
Dyad 3	518.17	0.0309	584.46	0.0908	508.66	0.0137	538.38	0.0039
Dyad 4	3547.98	0.0858	3408.76	0.2166	752.98	0.0230	538.40	0.0111

Table S2 Selected excitation wavelengths, λ , and oscillator strengths, f , for the optical transitions in presence of solvent (level: cc-pVDZ and LANL2DZ for Pd). Dipolar moment, μ , is also included.

NAME	TD-B97D								Experimental NIR (nm)
	CCl ₄				CHCl ₃				
	λ (nm)	f	μ (D)	COMPOSITIONS (%)	λ (nm)	f	μ (D)	COMPOSITIONS	
Dyad 1	634.84	0.0729	6.3	H→L (63.0)	634.84	0.0713	6.6	H→L (46.9)	---
Rhodamine 110 – MMA	3574.97	0.1248	40.7	H→L (71.2)	1924.14	0.0629	43.8	H→L (70.7)	---
Dyad 1a	660.91	0.0126	6.4	H→L (56.7)	662.64	0.0129	6.7	H→L (56.8)	---
Dyad 2	3157.32	0.2741	15.2	H→L (79.5)	3139.33	0.2728	18.3	H→L (78.2)	3100
Dyad 3	575.78	0.1293	9.2	H→L (45.0)	576.14	0.1229	9.9	H→L (58.9)	---
Dyad 4	3596.83	0.1178	44.3	H→L (71.0)	1832.46	0.0571	47.3	H→L (70.7)	3170



Scheme S5 Representation of dyads amide linker. Left and right parts correspond to the porphyrin and rhodamine moieties respectively. Inset: numbering of atoms.

Table S3 Ellipticity, ϵ , at the bond critical points of the C₁-C₂, C₂-O₃, C₂-N₄ and N₄-C₅ bonds of the amide linker of dyads along with $\Delta\epsilon$, the values corresponding to the differences between the dyads ϵ and those of their corresponding precursors. Atom numbering is given in Scheme S5.

Bond	ϵ						$\Delta\epsilon$					
	Rhodamine 110						Rhodamine 110					
	Dyad 1	- MMA	Dyad 1a	Dyad 2	Dyad 3	Dyad 4	Dyad 1	- MMA	Dyad 1a	Dyad 2	Dyad 3	Dyad 4
C ₁ -C ₂	0.11559	0.13855	0.11759	0.13555	0.11556	0.13841	-0.01823	0.00472	-0.01624	0.00175	-0.02251	0.00034
C ₂ -O ₃	0.11258	0.11625	0.11288	0.11873	0.11970	0.12140	-0.00333	0.00352	-0.00303	0.00282	-0.00010	0.00070
C ₂ -N ₄	0.13822	0.09405	0.13717	0.11678	0.14702	0.10598	-	-	-	-	-	-
N ₄ -C ₅	0.08369	0.09261	0.08421	0.09932	0.08950	0.09413	-0.01164	0.00466	-0.01112	0.01137	-0.00583	0.00618

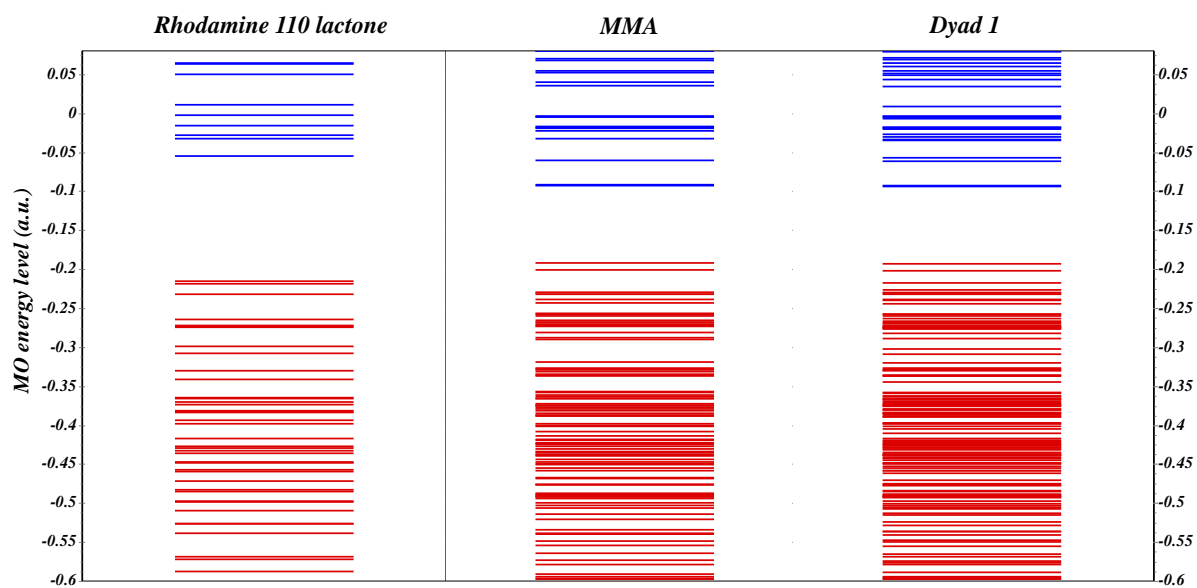


Figure S19A MOs energy levels of Rhodamine 110 lactone, MMA and of Dyad **1**.

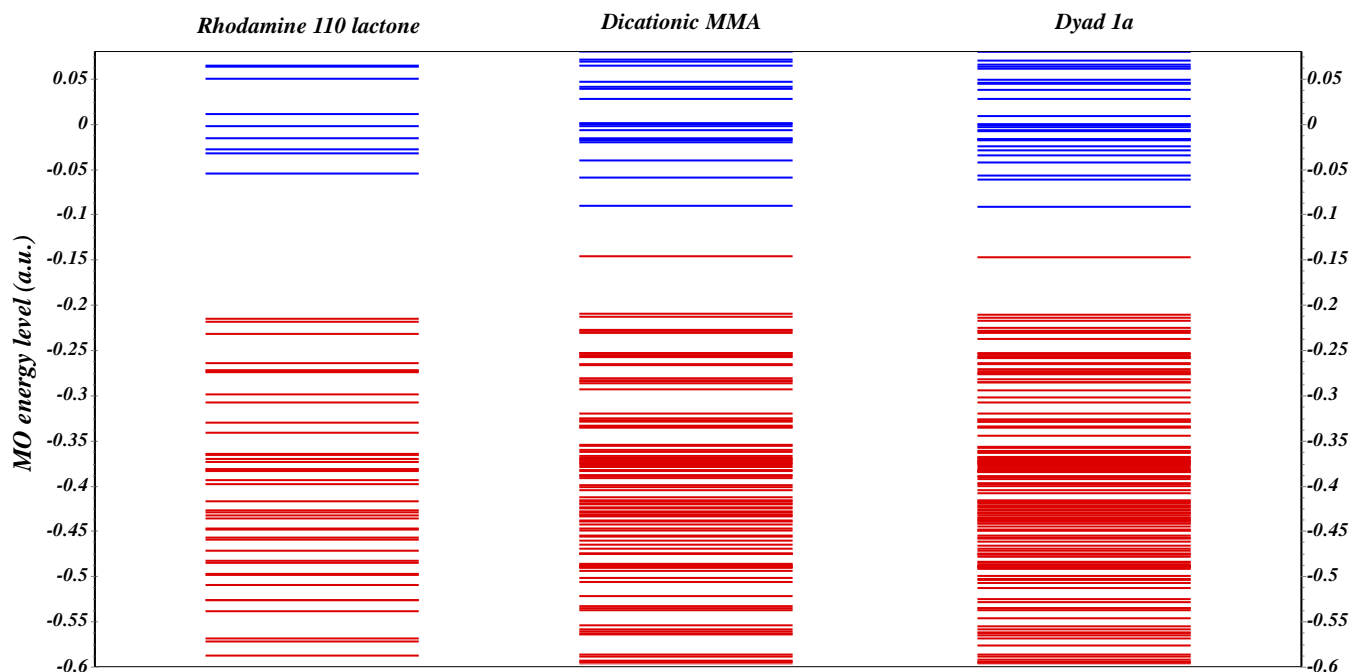


Figure S19B MOs energy levels of Rhodamine 110 lactone, dicationic MMA and of Dyad **1a**.

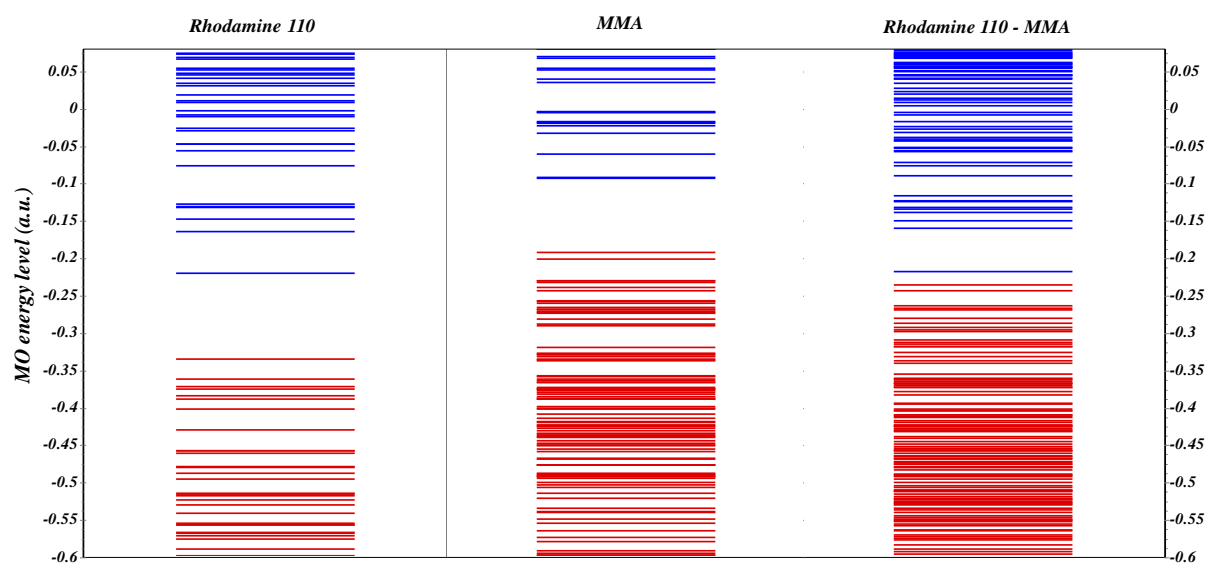


Figure S19C MOs energy levels of Rhodamine 110, MMA and of Rhodamine 110-MMA.

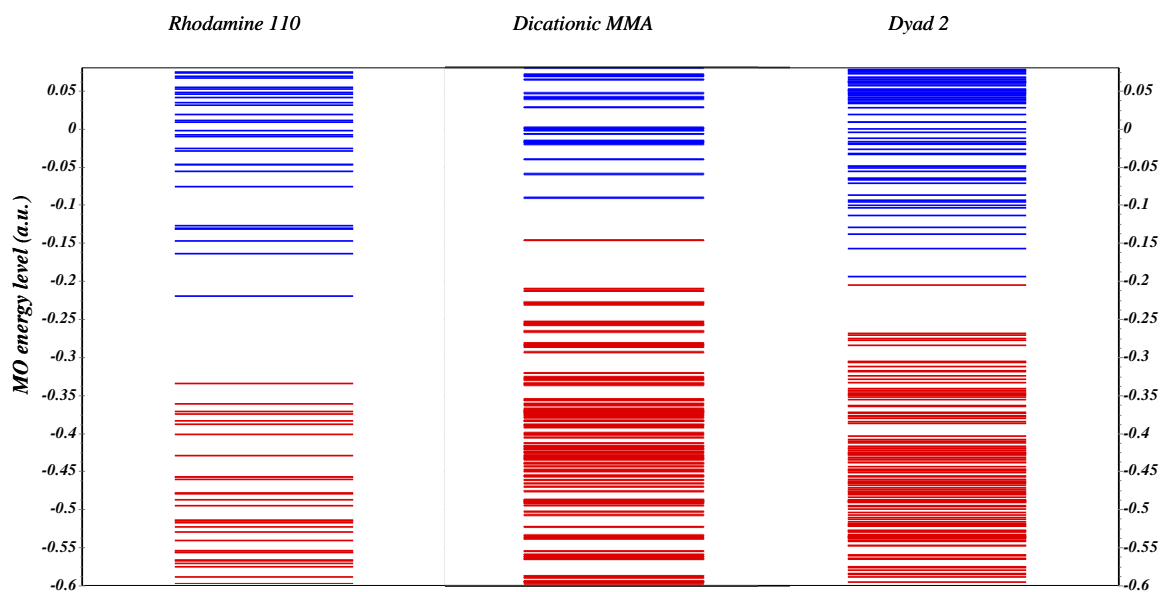


Figure S19D MOs energy levels of Rhodamine 110, dicationic MMA and of Dyad 2.

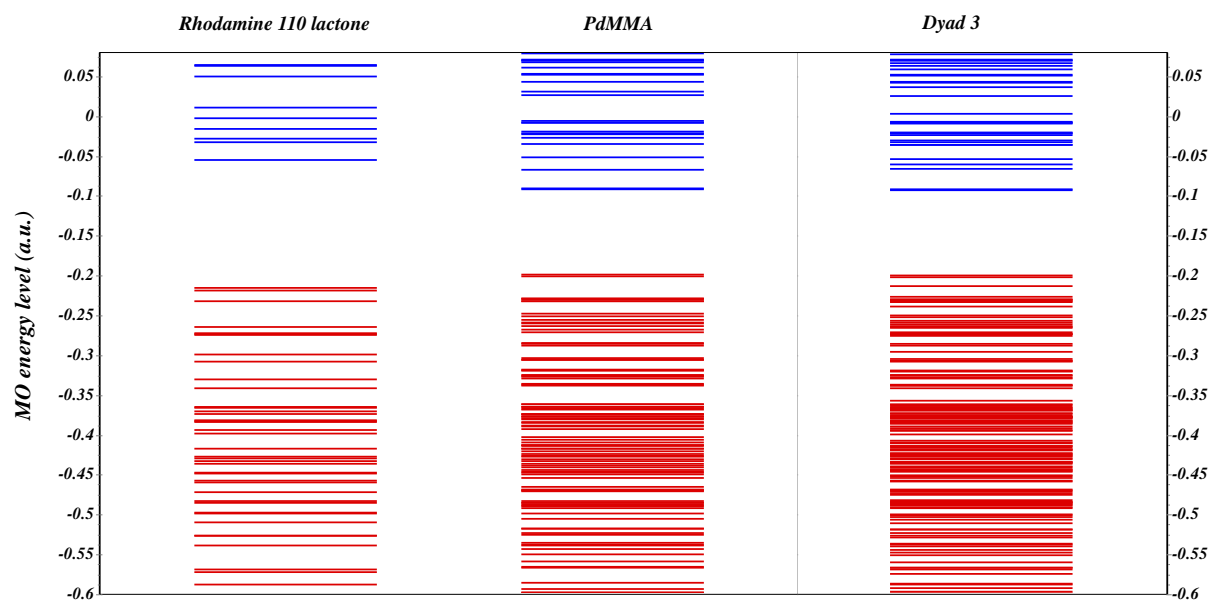


Figure S19E MOs energy levels of Rhodamine 110 lactone, PdMMA and of Dyad **3**.

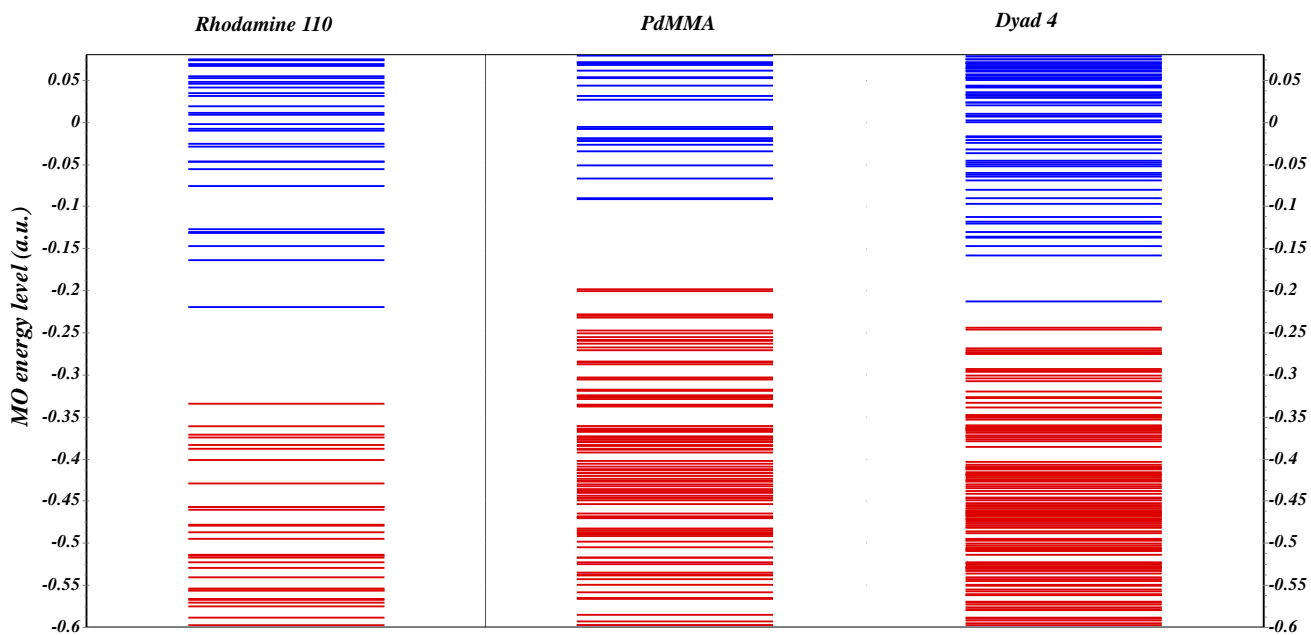


Figure S19F MOs energy levels of Rhodamine 110, PdMMA and of Dyad **4**.

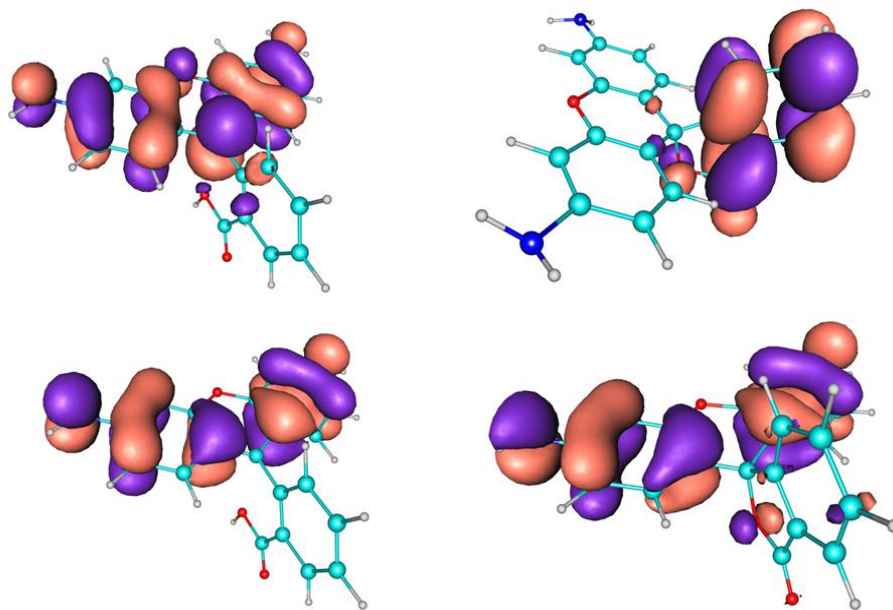


Figure S20 Rhodamine 110 (left) and Rhodamine 110 lactone (right) HOMOs (down) and LUMOs (up).

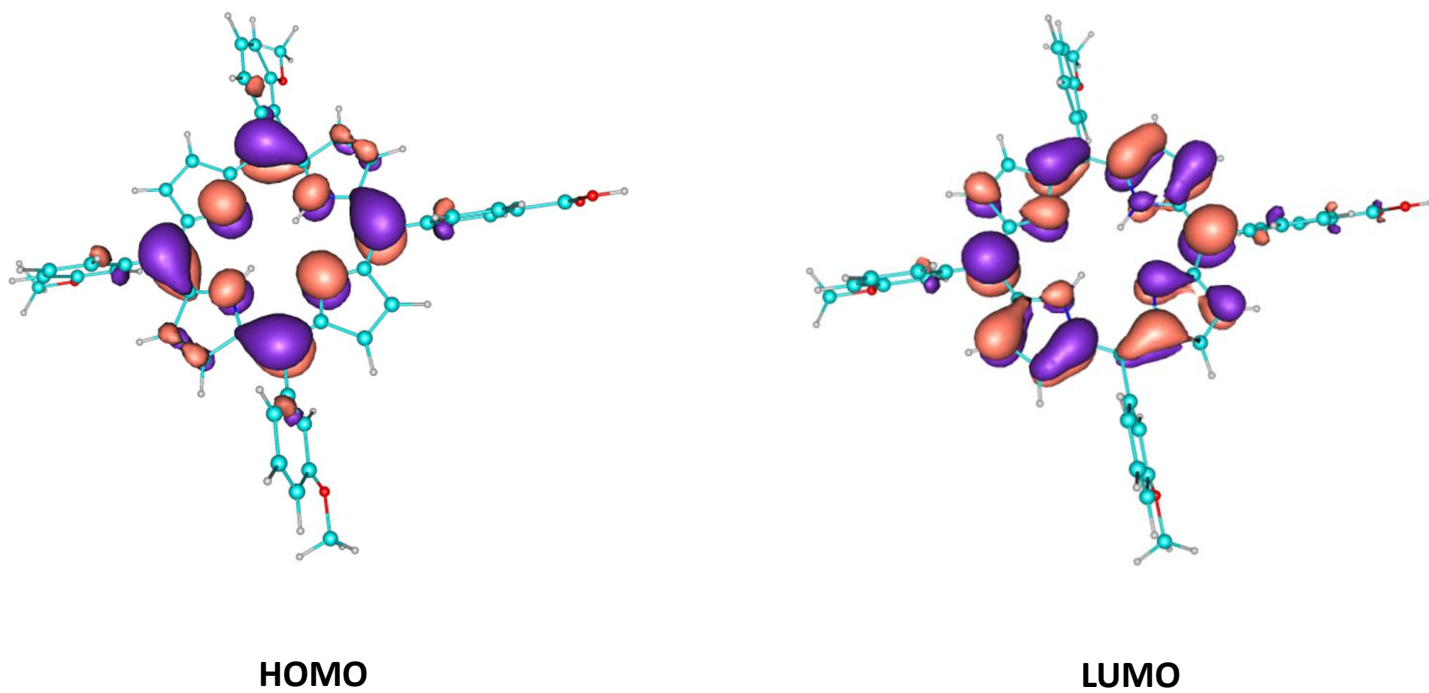


Figure S21 MMA HOMO and LUMO.

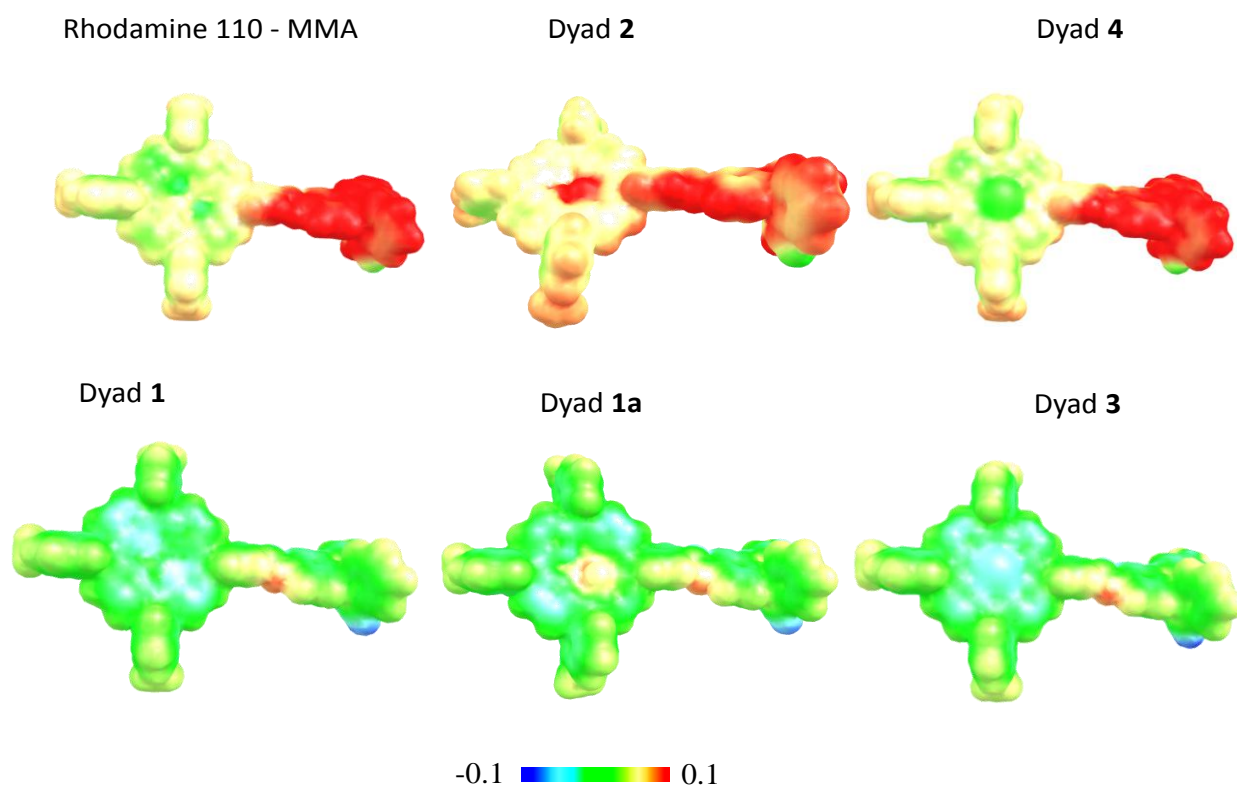


Figure S22 Molecular electrostatic potential of porphyrin-rhodamine dyads.

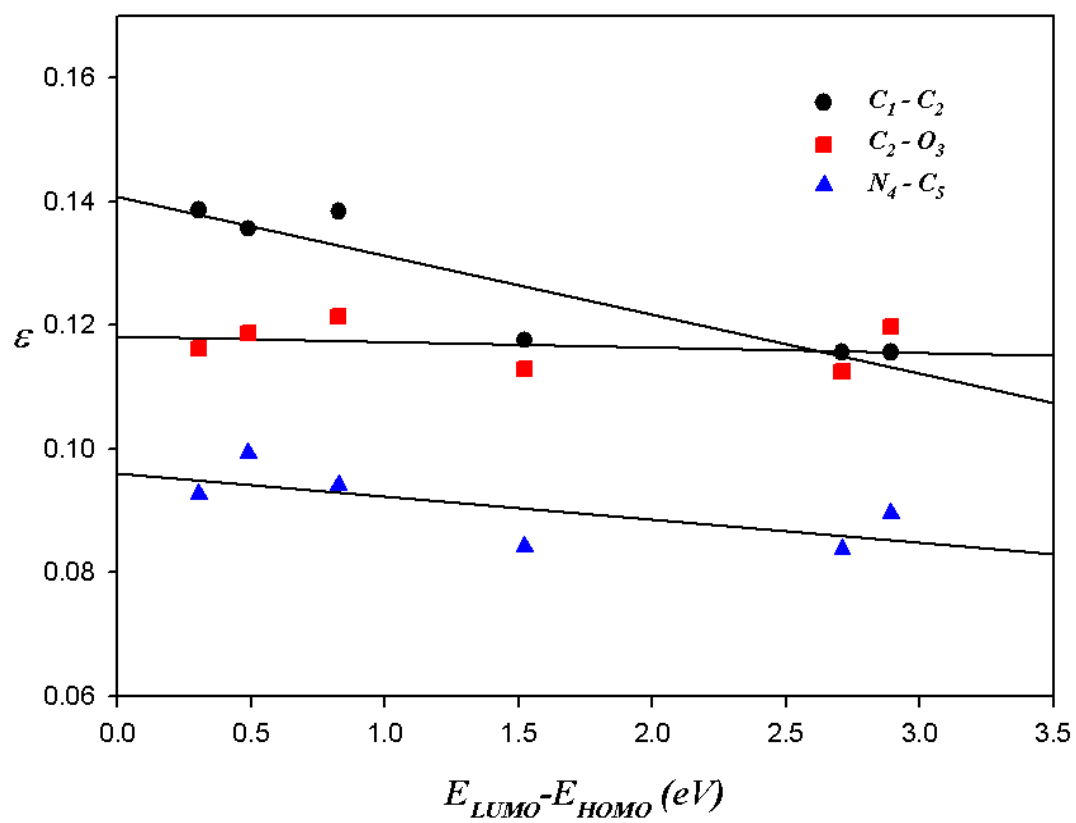


Figure S23 Correlation between ellipticities, ϵ , at the BCP with the band gap. Level of calculation: B3LYP/DGDZVP.

3 References

- 1 M. J. Frisch, G. W. Trucks, H. B. Schlegel, G. E. Scuseria, M. A. Robb, J. R. Cheeseman, G. Scalmani, V. Barone, B. Mennucci, G. A. Petersson *et al.* Gaussian 09, Revision A.1, Gaussian, Inc., Wallingford CT, 2009.
- 2 a) C. Lee, W. Yang, R. G. Parr, *Phys. Rev. B: Condens. Matter* 1988, **37**, 785. b) A. D. Becke *J. Chem. Phys.* 1993, **98**, 5648.
- 3 S. Grimme, Semiempirical GGA-type density functional constructed with a long-range dispersion correction *J. Comp. Chem.* 2006, **27**, 1787.
- 4 Y. D. Tew, and N. Handy, A new hybrid exchange-correlation functional using the Coulomb-attenuating method (CAM-B3LYP) *Chem. Phys. Lett.* 2004, **393**, 51.
- 5 H. Iikura, T. Tsuneda, T. Yanai, and K. Hirao, Long-range correction scheme for generalized-gradient-approximation exchange functionals *J. Chem. Phys.* 2001, **115**, 3540.
- 6 T. H. Dunning Jr., Gaussian basis sets for use in correlated molecular calculations. I. The atoms boron through neon and hydrogen *J. Chem. Phys.* 1989, **90**, 1007.
- 7 a) P. J. Hay and W. R. Wadt, *J. Chem. Phys.* 1985, **82**, 270. b) P. J. Hay and W. R. Wadt *J. Chem. Phys.* 1985, **82**, 284. c) P. J. Hay and W. R. Wadt *J. Chem. Phys.* 1985, **82**, 299.
- 8 a) N. Godbout, D. R. Salahub, J. Andzelm and E. Wimmer, *Can. J. Chem.* 1992, **70**, 560; b) C. Sosa, J. Andzelm, B. C. Elkin, E. Wimmer, K. D. Dobbs and D. A. Dixon *J. Phys. Chem.* 1992, **96**, 6630.
- 9 R. Teixeira, S. M. Andrade, V. V. Serra, P. M. R. Paulo, A. Sánchez-Coronilla, M. G. P. M. S. Neves, J. A. S. Cavaleiro and S. M. B. Costa. Reorganization of Self-Assembled Dipeptide Porphyrin J-Aggregates in Water–Ethanol Mixtures *J. Phys. Chem. B* 2012, **116**, 2396.
- 10 J. A. B. Ferreira, A. Sánchez-Coronilla, D. M. Togashi, H. Ferreira, J. R. Ascenso and S. M. B. Costa Electrophilic Reactivity of Tetrabromorhodamine 110 is Bromine Induced: Convergent Interpretation through Complementary Molecular Descriptors *J. Phys. Chem. A* 2012, **116**, 11938.
- 11 a) R. Bauernschmitt and R. Ahlrichs *Chem. Phys. Lett.* 1996, **256**, 454. b) M. E. Casida, C. Jamorski, K. C. Casida, D. R. Salahub, *J. Chem. Phys.* 1998, **108**, 4439.
- 12 a) E. Cancès, B. Mennucci and J. Tomasi *J. Chem. Phys.* 1997, **107**, 3032. b) B. Mennucci, E. Cancès, and J. Tomasi *J. Phys. Chem. B.* 1997, **101**, 10506.
- 13 a) R. F. Bader, *Atoms in Molecules – A Quantum Theory*, Oxford University Press, 1990. b) C. F. Matta and R. J. Boyd, (Eds.), *The Quantum Theory of Atoms in Molecules: From Solid State to DNA and Drug Design*, Wiley-VCH: Weinheim, 2007.
- 14 AIMAll (Version 11.08.23) Todd A. Keith Gristmill Software, Overland Park KS, USA, 2011 (aim.tkgristmill.com).
- 15 www.chemcraftprog.com

- 16 V. V. Serra, A. Zamarrón, M. A. F. Faustino, M. C. Iglesias-de la Cruz, A. Blázquez, J. M. M. Rodrigues, M. G. P. M. S. Neves, J. A. S. Cavaleiro, A. Juarran and F. Sanz-Rodríguez, New porphyrin amino acid conjugates: Synthesis and photodynamic effect in human epithelial cells *Bioorg. Med. Chem.* 2010, **18**, 6170.
- 17 M. Savarese, A. Aliberti, I. De Santo, E. Battista, F. Causa, P. A. Netti, and N. Rega, Fluorescence Lifetimes and Quantum Yields of Rhodamine Derivatives: New Insights from Theory and Experiment, *J. Phys. Chem. A* 2012, **116**, 7491.
- 18 (a) M. Gouterman In: Porphyrins; Dolphin, D. Ed.; Academic: New York, 1978; Vol. 3, pp 1-165. (b) M. Gouterman, Spectra of Porphyrins. *J. Mol. Spectrosc.* 1961, **6**, 138. (c) C. Weiss, H. Kobayashi, M. Gouterman. Spectra of porphyrins: Part III. Self-consistent molecular orbital calculations of porphyrin and related ring systems. *J. Mol. Spectrosc.* 1965, **16**, 415.
- 19 N. Santhanamoorthi, C.-M. Lo, and J.-C. Jiang Molecular Design of Porphyrins for Dye-Sensitized Solar Cells: A DFT/TDDFT Study *J. Phys. Chem. Lett.* 2013, **4**, 524.
- 20 R. Giovannetti The Use of Spectrophotometry UV-Vis for the Study of Porphyrins Macro To Nano Spectroscopy Edited by Jamal Uddin. Publisher: InTech, Published: June 29, 2012 Croatia.
- 21 G. De Luca, A. Romeo, L. Monsú-Scolaro, G. Ricciardi and, A. Rosa Siting-Atop Metallo-Porphyrin Complexes: Experimental and Theoretical Investigations on Such Elusive Species *Inorg. Chem.* 2009, **48**, 8493.
- 22 M. Presselt, B. Dietzek, M. Schmitt, S. Rau, A. Winter, M. Jäger, U. S. Schubert, and J. Popp A Concept to Tailor Electron Delocalization: Applying QTAIM Analysis to Phenyl-Terpyridine Compounds *J. Phys. Chem. A* 2010, **114**, 13163.